Review

Recent progress in the chemistry of heavy aromatics

By Shiori FUJIMORI,[*1] Yoshiyuki MIZUHATA[*1] and Norihiro TOKITOH[*1,†]

(Edited by Susumu KITAGAWA, M.J.A.)

Abstract: The aromaticity and synthetic application of "heavy benzenes", *i.e.*, benzenes containing a heavier Group 14 element (Si, Ge, Sn, and Pb) in place of skeletal carbon, have been the targets of many theoretical and synthetic studies. Although the introduction of a sterically demanding substituent enabled us to synthesize and isolate heavy aromatic species as a stable compound by suppressing their high reactivity and tendency to polymerize, the existence of a protection group is an obstruction to the development of functional materials based on heavy aromatics. This review will delineate the most recent topics in the chemistry of heavy aromatics, *i.e.*, the chemistry of "metallabenzenyl anions", which are the heavier Group 14 element analogs of phenyl anions stabilized by taking advantage of charge repulsion instead of steric protection.

Keywords: heavy aromatics, heavier Group 14 elements, kinetic stabilization, charge repulsion, metallabenzenyl anions, phenyl anion

1. Introduction

Aromatic compounds, *i.e.*, $[4n + 2]\pi$ electron ring systems, occupy a great part of organic chemistry and are widely studied from the viewpoints of not only fundamental chemistry but also materials chemistry. The history of aromatic compounds began with the isolation of benzene.[1)] Benzene was discovered in 1825 by Faraday,[2)] and its molecular formula was deduced as C_6H_6 by Mitscherlich in 1834.[3)] In 1865, Kekulé reported that benzene has a cyclic structure, where it should be "cyclohexatriene" bearing alternating single and double bonds (C–C: 1.47 Å; C=C: 1.34 Å).[4)] At this stage, however, two problems remained as unexplainable issues. The first one is the existence of only one isomer as the ortho-disubstituted benzene (*o*-xylene). Kekulé explained this issue using the concept of rapid equilibrium between two forms of benzene. The other is the higher stability of benzene compared with that of the chain-like conjugated polyene compounds toward addition reaction. The substitution reaction is more preferred to the addition reaction in the case of benzene. The latter problem could not be explained by the Kekulé's structure theory. In 1931, this problem was reasonably explained by the resonance theory reported by Pauling.[5)] Later, spectroscopic evidence showed that all bond lengths are equal and intermediate between the single and double carbon–carbon bond lengths (1.39 Å). It was also found that benzene is a planar molecule.[6)]

The detailed features of benzene are almost elucidated, and it is known as the most typical aromatic compound. Nowadays, so many types of compounds, in addition to benzene, are also known as aromatic compounds. Many definitions or criteria have been considered for characterizing **aromaticity** as follows:

(i) Structural criterion. The central ring system of aromatic compounds has a planar structure, along with bond lengths that are intermediate characters between single and double bonds. An aromaticity index based on bond lengths is the index Harmonic Oscillator Model of Aromaticity (HOMA).[7)] In the HOMA, a concept of the optimal bond length is proposed:

$$\mathrm{HOMA} = 1 - \left[\frac{\alpha}{n}\Sigma(R_{opt} - R_i)^2\right] \qquad [1]$$

where n is the number of bonds taken into the

[*1] Institute for Chemical Research, Kyoto University, Kyoto, Japan.
[†] Correspondence should be addressed to: N. Tokitoh, Institute for Chemical Research, Kyoto University, Gokasho, Uji, Kyoto 611-0011, Japan (e-mail: tokitou.norihiro.7e@kyoto-u.ac.jp).

doi: 10.2183/pjab.99.027

Fig. 1. HOMA values of benzenoid hydrocarbons. The bond lengths were determined using the X-ray diffraction technique.

summation and α is an empirical constant chosen to give HOMA = 0 for the hypothetical Kekulé structures of the typical aromatic systems and 1 for the system with all bonds equal to the optimal value R_{opt}. The individual bond lengths are depicted by R_i. The quantity R_{opt} is defined as a length of the CC bond for which the energy of the compression to the length of a double bond and expansion to the length of a single bond in 1,3-butadiene is minimal. For CC bonds, $\alpha = 257.7\,\text{Å}^{-2}$ and $R_{opt} = 1.388\,\text{Å}$. The HOMAs for principal benzenoid hydrocarbons and heterocyclic aromatic compounds are shown in Fig. 1.

(ii) Chemical behavior. Aromatic compounds undergo electrophilic substitution reactions more easily than addition reactions because the double bonds in the aromatic ring lose their reactivity as alkenes (C=C), azo compounds (N=N), imine (C=N), and sulfoxide (S=O).

(iii) Magnetic criterion. Aromatic compounds have a large ring current effect, along with unique magnetic features such as anisotropic effect in chemical shifts, large magnetic anisotropy, and diamagnetic susceptibility exaltation. An aromaticity index called nucleus-independent chemical shift (NICS) has been introduced by Schleyer *et al.*[8] It is defined as a value of the absolute shielding computed at a ring center or some other interesting points of the system. A ring with negative NICS values qualifies as aromatic, and the more negative the NICS is, the more aromatic is the ring. Consequently, antiaromatic systems have large positive NICS. Nonaromatic systems show a small absolute value of NICS. NICS(0) (*i.e.*, at the ring center) and NICS(1) (*i.e.*, at points 1 Å above the ring center) for several typical π-electron systems are presented in Fig. 2.[9]

(iv) Energetic criterion. The stability of an aromatic ring is enhanced because of the large resonance energy. The ideas of isodesmic[10] and homodesmotic[11] reactions gave very effective methods for the estimation of various stabilization energies, including those of aromatic systems, called

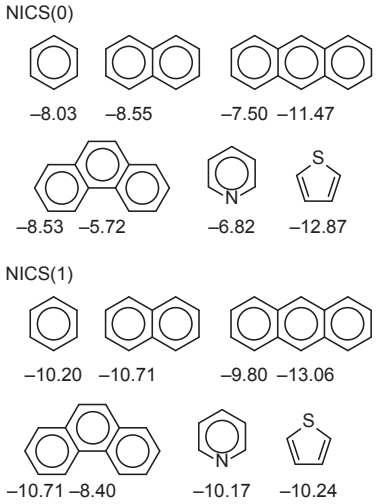

Fig. 2. Upper: NICS(0) values calculated at the RB3LYP/6-311G** level. Lower: NICS(1) values calculated at the RB3LYP/6-311G** level.

the aromatic stabilization energy. Such stabilization can be measured experimentally or estimated theoretically.

Although aromaticity has been extensively studied for more than a century, there is no generally acceptable definition yet.[12] Therefore, the aromaticity of the compounds should be evaluated carefully by considering all criteria described above.

2. Aromatic compounds containing heavier Group 14 elements

2.1. Generation of silabenzene and germabenzene. A number of reactive intermediates have been studied in the gas phase and/or low-temperature matrices. Among them, there are some reports of spectroscopic observation of neutral sila- and germaaromatic compounds as transient species using these methods.

The first spectroscopic observation of silabenzene was reported in 1980.[13] Silabenzene **1** was generated by the flash vacuum pyrolysis of the corresponding allylsilane. The generation of **1** was suggested by the measurement of the photoelectron spectrum in the gas phase and the UV and IR spectra in low-temperature Ar matrices (Scheme 1, left). Silabenzene **1** was also generated by the pyrolytic dehydrogenation of 1-silacyclohexa-2,5-diene and detected by the UV and IR spectra in low-temperature matrices (Scheme 1, right).[14]

In 1980, silabenzene **3a** and germabenzene **3b** bearing two *t*-Bu groups on their 1,4-positions were

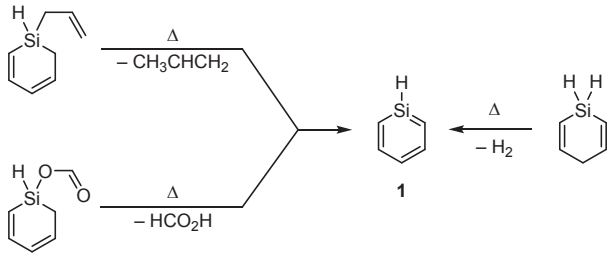

Scheme 1. Generation of silabenzene **1**.

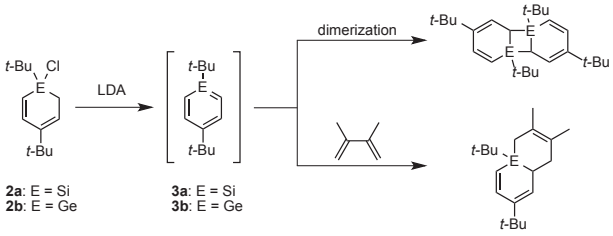

Scheme 2. Generation of sila- and germabenzenes **3a** and **3b**.

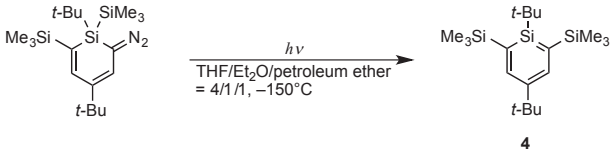

Scheme 3. Synthesis of silabenzene **4**.

generated by the reaction of the corresponding chlorosilane **2a** or chlorogermane **2b** with LDA (Scheme 2).[15] The generation of **3a** and **3b** was confirmed by the formation of their [2 + 2] dimer and the trapping reactions with diene, but no description was made for their spectroscopic properties. In addition, the facile dimerization of **3a** and **3b** even with two *t*-Bu groups indicates that silabenzene and germabenzene are highly liable to undergo self-dimerization.

In 1988, the synthesis of silabenzene **4** bearing two *t*-Bu and two trimethylsilyl groups *via* a photochemical reaction was reported by Märkl *et al.* (Scheme 3).[16] However, silabenzene **4** is stable only below −100 °C in a special combination of solvents (THF/ether/petroleum ether).

In 1989, silabenzene **5** bearing bulkier substituents was synthesized by the thermal desorption of the corresponding methoxysilane under Ar flow. Silabenzene **5** is stable only below −180 °C (Scheme 4).[17]

As mentioned above, **heavy benzenes** had been considered transient and unisolable compounds for a long time due to their high reactivity and

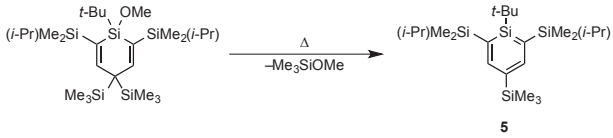

Scheme 4. Synthesis of silabenzene **5**.

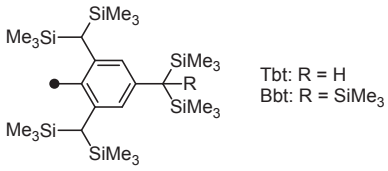

Fig. 3. Extremely bulky aryl groups Tbt and Bbt.

tendency to polymerize and their structural and chemical properties had not been revealed.

2.2. Stabilization by bulky aryl groups. As mentioned in Section 1.1, heavy benzenes are highly reactive and difficult to be isolated under ambient conditions because their π-bonds are generally weak and highly reactive because of the poor overlap of the p orbitals between carbon and heavier Group 14 atoms.[18] To stabilize such highly reactive compounds, kinetic stabilization has been utilized. Kinetic stabilization does not strongly affect the structures and properties of the double bond between heavier main group elements, and thus, one can investigate the intrinsic character of the heavier double-bond compounds using kinetic stabilization methods.

In this context, Tokitoh *et al.* developed the 2,4,6-tris[bis(trimethylsilyl)methyl]phenyl (Tbt) and 2,6-bis[bis(trimethylsilyl)methyl]-4-[tris(trimethylsilyl)methyl]phenyl (Bbt) groups for the kinetic stabilization of highly reactive compounds (Fig. 3).[19] It has been revealed that the compounds bearing the Tbt or Bbt group have enough reaction space around the core functional group, although they are extremely bulky substituents bearing six or seven trimethylsilyl groups.[20]

The development of the protecting groups made it possible to synthesize and isolate a variety of highly reactive compounds containing heavier main group elements, particularly triple-bond compounds between heavier Group 14 elements **6**[21] and double-bond compounds between heavier Group 15 elements **7**[22] bearing only one substituent at each heavier element. In addition, disilenes **8**[23] having small alkynyl substituents and a series of heavy ketones **9**,[24] which are double-bond compounds between

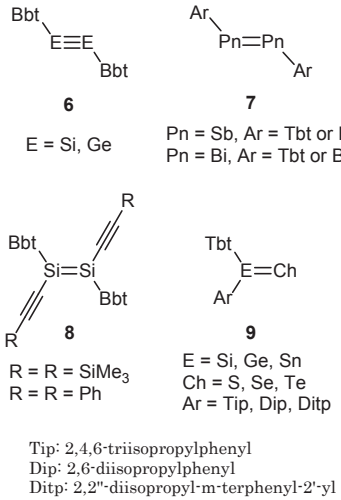

Fig. 4. Kinetically stabilized heavy double- and triple-bond compounds.

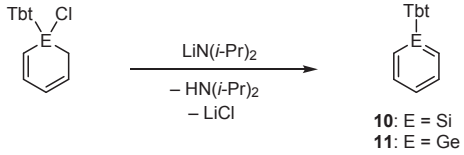

Scheme 5. Synthesis of sila- and germabenzenes **10** and **11**.

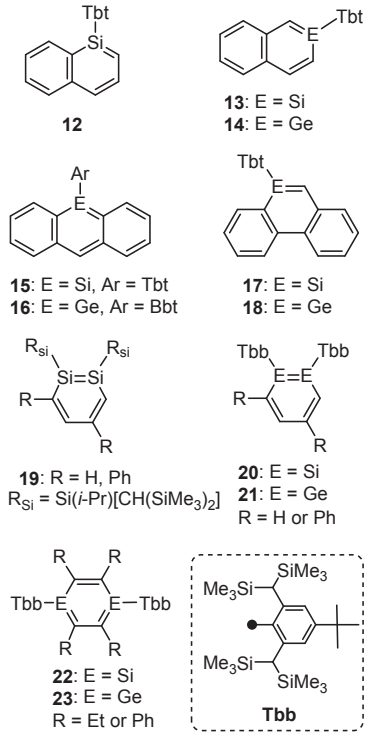

Fig. 5. Examples of the isolated polycyclic aromatic hydrocarbons containing silicon or germanium atoms, disilabenzenes, and digermabenzenes.

heavier Group 14 and 16 elements and could not be substituted on the Group 16 element, were successfully synthesized (Fig. 4).

2.3. Stable heavy aromatics. In contrast to the cases of multiply bonded systems mentioned above, no stable neutral aromatic compounds containing a heavier Group 14 element under ambient conditions had been reported until the year 2000. The first stable silabenzene **10**[25] and germabenzene **11**[26] have been synthesized and isolated by utilizing an extremely bulky substituent, the Tbt group (Scheme 5).

In ^{1}H and ^{13}C NMR spectroscopy, all signals of the sila- and germabenzene rings were observed in the aromatic region. In addition, the molecular geometries of **10** and **11** were determined by X-ray crystallographic analysis. Their structural analysis revealed the completely planar geometries around the silicon and germanium atoms and the planarity of the sila- and germabenzene rings. Moreover, the lengths of the two E–C bonds (E = Si, Ge) and the four C–C bonds in the ring were almost the same, and they were between those of the corresponding double and single bonds. Thus, these results strongly support that **10** and **11** have delocalized 6π-electron ring systems and an aromatic character. Furthermore, Yamashita *et al.* reported the synthesis, structure, and electronic properties of monomeric germabenzenes and a stannabenzene stabilized by two ortho-Si(*i*-Pr)$_3$ groups in 2019.[27]

In addition, polycyclic aromatic hydrocarbons containing a heavier Group 14 element (Si and Ge)[28] **12**–**18**, 1,2-disilabenzenes **19**[29a] and **20**,[29b] and 1,2-digermabenzenes **21**[30] have been synthesized by utilizing kinetic stabilization, and their aromatic character has been revealed. More recently, we have expanded this chemistry to that of 1,4-dimetallabenzenes **22**[31] and **23**[32] (Fig. 5).

2.4. Ionic heavy aromatics. A number of ionic aromatic compounds containing a heavier Group 14 element have been known, and very few neutral aromatic compounds containing a heavier Group 14 element have been synthesized and isolated by taking advantage of an extremely bulky substituent. In particular, cyclopentadienide analogs, where one carbon atom of a cyclopentadienide ion is replaced with a heavier Group 14 element, have been well investigated since the 1990s, and the synthesis and

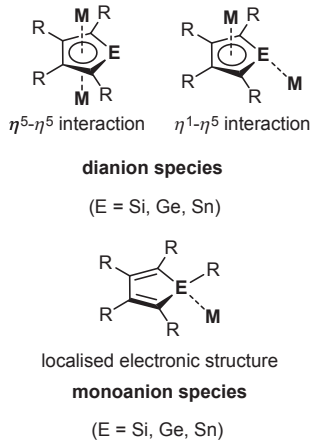

Fig. 6. Structures of mono- and dianions of Group 14 metalloles.

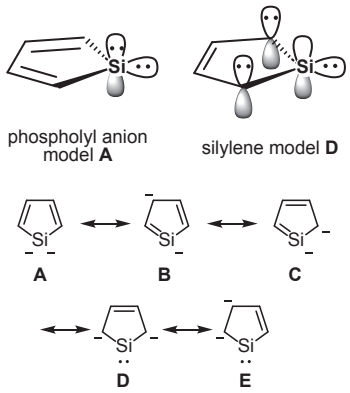

Fig. 7. Resonance structures for silole dianion.

isolation of many mono-[33] and dianions[34] of Group 14 metalloles (1-metallacyclopentadienes) have been reported. These species are thermally stable, and some of them are structurally characterized by X-ray crystallographic analyses. The dianion species have an η^5–η^5 or η^1–η^5 interaction mode in their complexes, and the endocyclic C–C bond lengths are almost the same in all cases, indicating their π-electron-delocalized structures (Fig. 6). In contrast to the case of the dianion species, monoanion species are known to show localized electronic structures.

In 1990, the first silole dianion **25** was synthesized by the reaction of 1,1-dichlorosilole **24** with sodium by Joo *et al.* (Scheme 6, left).[35] The generation of **25** was confirmed by ^{1}H and ^{13}C NMR spectroscopy and the trapping reactions with methyl iodide or with trimethylchlorosilane. Furthermore, Boudjouk *et al.* reported the synthesis of silole dianion **26** by the reaction of **24** with lithium, together with its ^{1}H, ^{13}C, and ^{29}Si NMR data in 1994 (Scheme 6, right).[36] Later, the X-ray structure of **26** was established by West *et al.*[37]

The ^{29}Si NMR spectrum of silole dianion **26** showed only one resonance at 68.54 ppm, which was remarkably downfield-shifted compared with that of the starting material **24** (6.80 ppm). In the ^{13}C NMR spectrum of **26**, the signals for the C_α and C_β atoms in the ring were observed in the upfield region. The upfield shifts for C_α and C_β in the ^{13}C NMR spectrum and the downfield shift in the ^{29}Si NMR spectrum were consistent with significant charge delocalization from the silicon onto the ring. The structure of **26** contained two different lithium atoms. One lithium atom was bound to the silole ring with an η^5-fashion, and the other was bound to the silicon atom with an η^1-fashion. Moreover, the three C–C bond lengths in the ring were nearly equal. These results of the spectroscopic and X-ray crystallographic analyses indicate that **26** has an aromatic character.

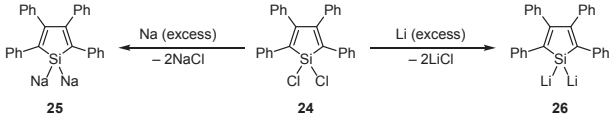

Scheme 6. Synthesis of silole dianions **25** and **26**.

As shown in Fig. 7, resonance structures **A**–**E** were proposed for the electronic structure of silole dianion.[38] Among them, reasonable models for understanding the electronic structure of **26** are phospholyl anion model **A**, where the negative charges are localized on the silicon atom, and cyclic silylene models **D** and **E**, where the negative charges are delocalized on the silole ring carbons. The upfield shifts in ^{13}C NMR and the downfield shift in ^{29}Si NMR indicate that the resonance structures of cyclic silylene models **D** and **E** are the major contributor in **26**. In cyclic silylene models **D** and **E**, the silicon atom shares nearly pure p orbitals with the neighboring carbon atoms and has an s orbital to hold a lone pair.

Since then, silole dianion **27**[38] and germole dianions **28**[39),40] and **29**[41] were synthesized and characterized by NMR spectroscopic and X-ray crystallographic analyses. Furthermore, other ionic aromatic compounds containing heavier Group 14 elements, such as cyclotrisilenium cation **30**,[42] cyclotrigermenium cation **31**,[43] sila- and germafluorene dianions **32** and **33**,[44] and 1,2-disila-3-germacyclopentadienide **34**,[45] were successfully synthesized and characterized (Fig. 8).

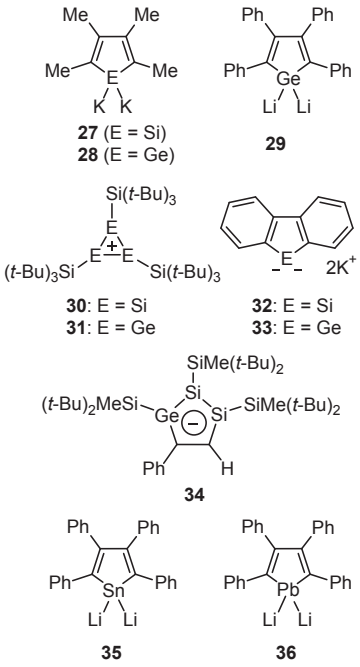

Fig. 8. Stable ionic aromatic compounds containing heavier Group 14 elements.

Not only silicon and germanium but also tin and lead analogs, *i.e.*, stannole dianion **35**[46] and plumbole dianion **36**,[47] were synthesized and isolated by Saito *et al.* (Fig. 8). X-Ray crystallographic analysis revealed their planar structures with no alternation of carbon–carbon bond lengths in the five-membered-ring cores. Their NMR spectra and relativistic theoretical calculations showed a considerable aromatic character in the molecule.

2.5. New perspective in heavy aromatics chemistry. As described above, it has been proved that highly reactive heavy aromatics can be synthesized and isolated as stable compounds by taking advantage of appropriate protection and they are not elusive but they exist as molecules capable of handling under ambient conditions. However, heavy aromatics with full kinetic stabilization are inappropriate for further modification and/or transformation and it is difficult to utilize them as a useful building block for more sophisticated molecular systems.

Therefore, we next examined the creation of synthetically more useful tools of heavy aromatics, *i.e.*, "**heavy phenyl anions**". Because many ionic heavy aromatics have been successfully synthesized as stable compounds as mentioned above, we expected that the heavier Group 14 element analogs of aryl anions might also be stabilized by charge repulsion instead of steric protection (Fig. 9).

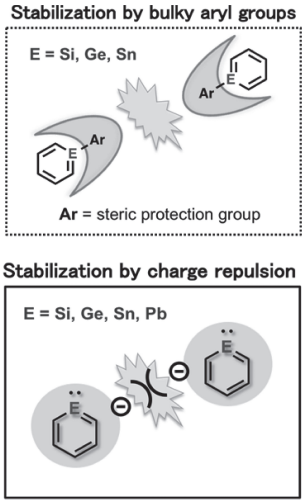

Fig. 9. Stabilization by bulky aryl groups and charge repulsion of heavier benzene derivatives.

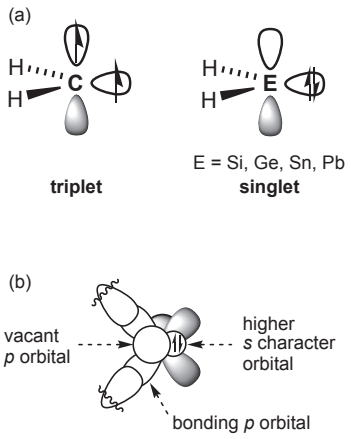

Fig. 10. (a) Difference between the ground states of carbenes and metallylenes; (b) the ground state of metallylenes.

In contrast to the carbon atom, the heavier Group 14 atoms have a low ability to form hybridized orbitals. They therefore prefer the $(ns)^2(np)^2$ valence electron configurations in their divalent species. Because two electrons remain as a singlet pair in the ns orbital, the ground state of H_2M: (M = Si, Ge, Sn, Pb) is a singlet, unlike the case of H_2C:, where the ground state is a triplet (Fig. 10).

Therefore, **heavy phenyl anions** are expected to exhibit characters of not just aromatic compounds but also divalent species, the contribution of which is negligible in the parent phenyl anion. Moreover, **heavy phenyl anions** could be available as a building block for the introduction of a **heavy benzene** moiety by both nucleophilic and insertion reactions.

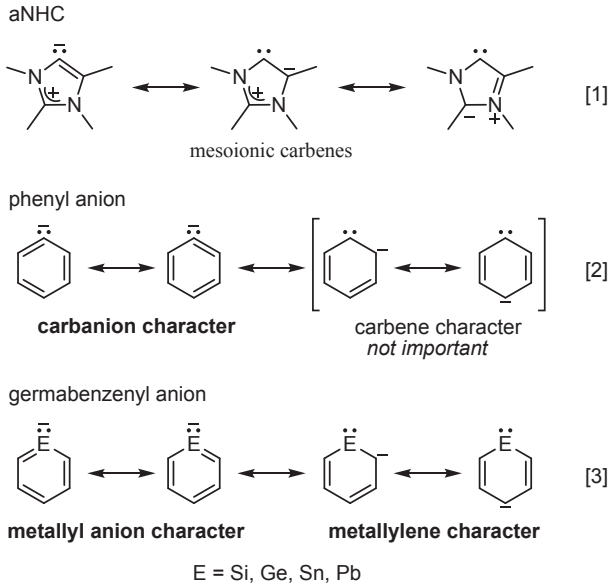

Fig. 11. Resonance structures for mesoionic carbenes (eq. 1), the phenyl anion (eq. 2), and metallabenzenyl anions (eq. 3).

3. Germabenzenyl anion: A germanium analog of a phenyl anion

3.1. Phenyl anions. The target compound is the heavier Group 14 element analog of phenyl anions. Phenyl anions, *i.e.*, metallated benzenes such as phenyllithium, are commonly used organometallic reagents in addition, substitution, and metallation reactions. The resonance forms of phenyl anions (Fig. 11, eq. 2) should be drawn as localized anions with delocalized π-electrons (aromatic character), and the contribution from a delocalized anion charge with a carbene center is negligible. Recently, mesoionic carbenes (MICs), also referred to as abnormal or remote *N*-heterocyclic carbenes (aNHCs and rNHCs, respectively), have been widely investigated and reviewed.[48] In essence, MICs act as neutral and strong σ-donor carbene ligands, whereby the canonical forms with a carbene center and a delocalized anion (and cation) offer a larger contribution to the resonance forms (Fig. 11, eq. 1). Meanwhile, the stability of the divalent state of the Group 14 elements relative to the tetravalent state increases upon descending the periodic table (Si, Ge, Sn, and Pb) due to the $(ns)^2(np)^2$ valence electron configuration, which is preferred by the heavier homologs of Group 14.[49] Thus, the replacement of an anionic carbon atom with a heavier Group 14 element in phenyl anions could result in the enhancement of the divalent (metallylene) character and could render phenyl anion analogs with an ambident character between a localized (metallyl) anion with an aromatic backbone and a divalent center (metallylene) with a delocalized anion charge (*cf.* MICs) accessible (Fig. 11, eq. 3).

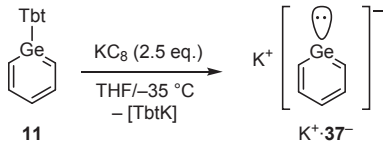

Scheme 7. Synthesis of germabenzenylpotassium $K^+\cdot\mathbf{37}^-$.

On the basis of this information mentioned above, we synthesized **heavy phenyl anions** by the reaction of neutral heavy benzenes bearing a bulky aryl group with some reducing agents. As the first target, germanium was chosen as a center element because its electronegativity (electronegativity: 1.90 for Si, 2.01 for Ge, and 1.96 for Sn)[50] is the highest among silicon, germanium, and tin. In this section, we describe the synthesis of the germanium analog of the phenyl anion called germabenzenyl anion, which exhibits significant contributions from both germylene and aromatic resonance structures.

3.2. Synthesis.[51),52] At first, we attempted to synthesize parent germabenzenylpotassium $K^+\cdot\mathbf{37}^-$ by the reductive aryl elimination of 1-Tbt-germabenzene **11**[26] with KC_8 (Scheme 7). The generation of $K^+\cdot\mathbf{37}^-$ was strongly indicated by the signals in the ^{1}H NMR spectrum with chemical shifts (6.35, 7.51, and 8.96 ppm) and with the reasonable couplings and integral values. Compound $K^+\cdot\mathbf{37}^-$, however, could not be isolated because of its poor crystallinity and gradual decomposition in solution. Hence, to synthesize and isolate a stable germabenzenyl anion, we introduced a *tert*-butyl group on the carbon atom adjacent to the germanium atom of the 1-Tbt-germabenzene skeleton.

Thus, as a starting compound for germabenzenyl anion $\mathbf{39}^-$, 2-*tert*-butyl-1-Tbt-germabenzene **38**[51] was synthesized (Scheme 8). The molecular structure and aromaticity of germabenzene **38** were reasonably established based on the NMR and UV–vis spectra, X-ray crystallographic analysis, and theoretical calculations.

The reaction of **38** with 2.5 equivalents of potassium graphite in THF resulted in the formation of germabenzenylpotassium $K^+\cdot\mathbf{39}^-$ in 93% yield (Scheme 9).[51] $K^+\cdot\mathbf{39}^-$ was isolated as a yellow solid, which was insoluble in hydrocarbon solvents such as *n*-hexane, benzene, and toluene. Although $K^+\cdot\mathbf{39}^-$ is

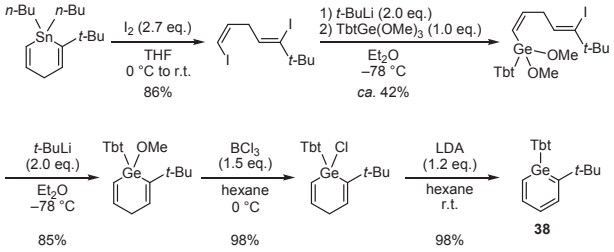

Scheme 8. Synthesis of germabenzene **38**.

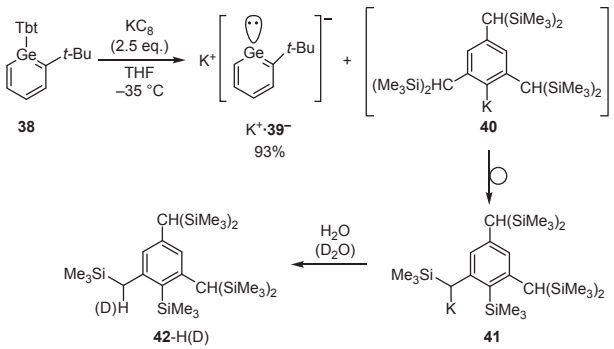

Scheme 9. Synthesis of germabenzenylpotassium $K^+ \cdot \mathbf{39}^-$.

highly moisture-sensitive, it has high thermal stability under an inert atmosphere in the solid state [mp 315 °C (decomp.)] and in THF-d_8 solution. The Tbt moiety was extruded as benzylpotassium **41** mainly in the filtrate of the reaction mixture, where it could be trapped with D_2O and H_2O. Although the formation mechanism of **41** is still unclear, initially formed TbtK **40** would undergo a 1,3-silyl shift as in the case of TbtLi[53] or rearrangement and elimination from the resulting anionic species that occurred at the same time. A number of reductive cleavages of a substituent (mainly aryl) on a Group 14 element have been reported for the generation of heavier analogs of vinyl anion[54] and cyclopentadienide.[46c),47),55]

Considering that the starting material was completely converted into $K^+ \cdot \mathbf{39}^-$ and **41**, germabenzene **38** should accommodate two electrons during the reduction. When **38** was reduced with an equimolar amount of potassium graphite, a 1:1 mixture of $K^+ \cdot \mathbf{39}^-$ and **38** was obtained (Scheme 10). The result suggests that the second one-electron reduction, together with the elimination of **41**, should be faster than the first one-electron reduction. Single crystals of $K^+ \cdot \mathbf{39}^-$ suitable for X-ray diffraction analysis were obtained from slow recrystallization in THF.

In addition, treatment of $K^+ \cdot \mathbf{39}^-$ with an excess of 18-crown-6 or an equimolar amount of crypt-222 in

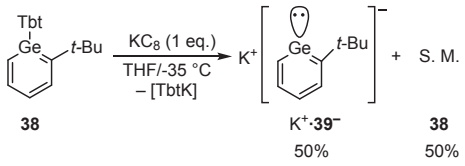

Scheme 10. Reaction of germabenzene **38** with potassium graphite.

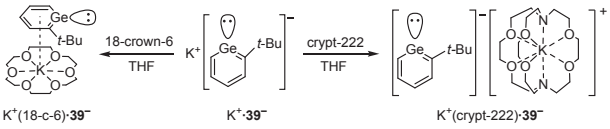

Scheme 11. Complexation of $K^+ \cdot \mathbf{39}^-$ with macrocyclic ethers.

THF afforded K^+(18-c-6)·$\mathbf{39}^-$ and K^+(crypt-222)·$\mathbf{39}^-$, respectively (Scheme 11). In contrast to $K^+ \cdot \mathbf{39}^-$, K^+(18-c-6)·$\mathbf{39}^-$ and K^+(crypt-222)·$\mathbf{39}^-$ were soluble in benzene and toluene and were insoluble in hexane. The single crystals of K^+(18-c-6)·$\mathbf{39}^-$ and K^+(crypt-222)·$\mathbf{39}^-$ suitable for X-ray diffraction analysis were obtained by slow recrystallization from benzene.

As in the case of germabenzenylpotassium $K^+ \cdot \mathbf{39}^-$, treatment of **38** with 2 equivalents of lithium naphthalenide in THF at −35 °C afforded germabenzenyllithium $Li^+ \cdot \mathbf{39}^-$.[52] $Li^+ \cdot \mathbf{39}^-$ was thermally unstable even under an inert atmosphere and gradually decomposed during 24 h in THF solution to give unidentified compounds. Therefore, the isolation of $Li^+ \cdot \mathbf{39}^-$ was not achieved and its structural determination and measurement of ^{13}C NMR spectrum were not performed. Its formation was confirmed by the ^1H NMR spectrum (^1H NMR yield of $Li^+ \cdot \mathbf{39}^-$: 67%), and the ^1H NMR measurement of this crude mixture showed the formation of $Li^+ \cdot \mathbf{39}^-$ along with naphthalene, compound **42**-H, and an unidentified compound (Scheme 12).

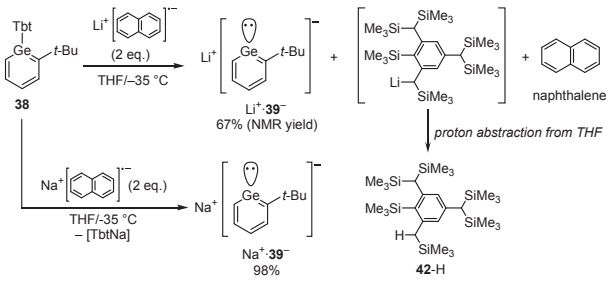

Scheme 12. Synthesis of germabenzenylmetals $Li^+ \cdot \mathbf{39}^-$ and $Na^+ \cdot \mathbf{39}^-$.

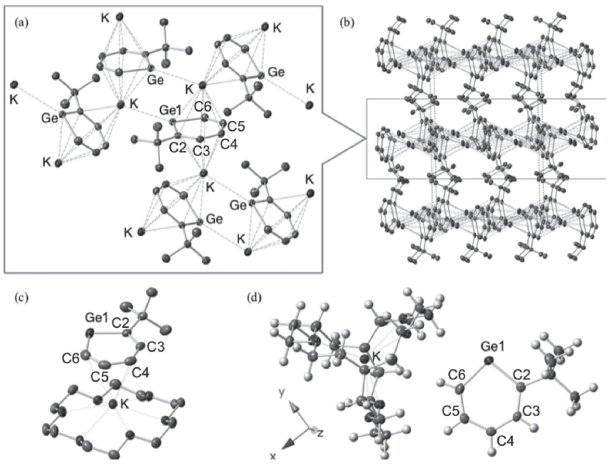

Fig. 12. Atomic displacement parameter plots for K^+·**39**$^-$ (a), K^+(18-c-6)·**39**$^-$ (c), and K^+(crypt-222)·**39**$^-$ (d) with thermal ellipsoids set at 50% probability; crystal packing for K^+·**39**$^-$ (b); all hydrogen atoms were omitted for clarity. (*Angew. Chem. Int. Ed.* **2017**, *56*, 4588–4592)

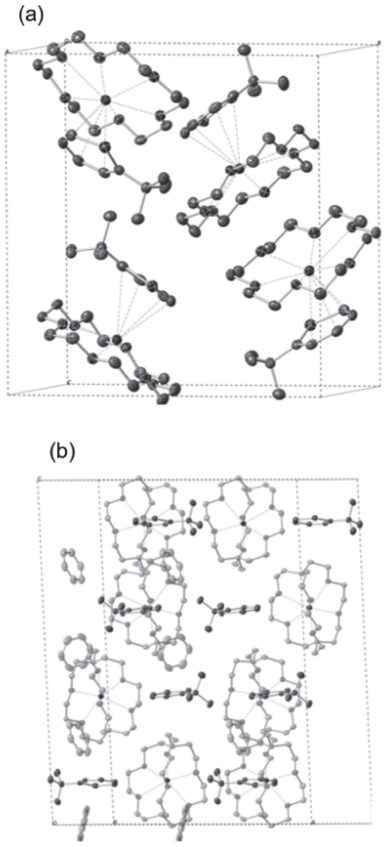

Fig. 13. Crystal packing of K^+(18-c-6)·**39**$^-$ (a) and K^+(crypt-222)·**39**$^-$·benzene (b) with atomic displacement parameters set at 50% probability. (*Angew. Chem. Int. Ed.* **2017**, *56*, 4588–4592)

The reaction of **38** with 2 equivalents of sodium naphthalenide under the same conditions as above afforded Na^+·**39**$^-$ in 98% isolated yield (Scheme 12).[52] Like the case of K^+·**39**$^-$, germabenzenylsodium Na^+·**39**$^-$ had high thermal stability under an inert atmosphere in the solid state [mp 220 °C (decomp.)] and in THF-d_8 solution, though it is highly moisture-sensitive.

3.3. X-Ray diffraction studies.[51),52)] The molecular structures of K^+·**39**$^-$, K^+(18-c-6)·**39**$^-$, and K^+(crypt-222)·**39**$^-$ are shown in Fig. 12. In addition, crystal packing of K^+(18-c-6)·**39**$^-$ and K^+(crypt-222)·**39**$^-$ is shown in Fig. 13.

It should be noted that no X-ray structural analyses have been reported on arylpotassium compounds to date. The crystal packing of K^+·**39**$^-$ exhibited a layer structure in which the potassium atoms were coordinated in an η^1-fashion to the germanium atom and in an η^6-fashion to the germabenzenyl ring. In K^+(18-c-6)·**39**$^-$, each ion pair was isolated even though a π-type interaction between the potassium atom and the germabenzenyl moiety was observed. By contrast, the germabenzenyl moieties in K^+(crypt-222)·**39**$^-$ were separated from the potassium ions and the shortest Ge–K distance observed was approximately 6 Å, which was longer than the sum of the corresponding van der Waals radii (*ca.* 4.85 Å).[56]

The selected bond lengths and angles for K^+·**39**$^-$, K^+(18-c-6)·**39**$^-$, K^+(crypt-222)·**39**$^-$, and **38** are summarized in Fig. 14.

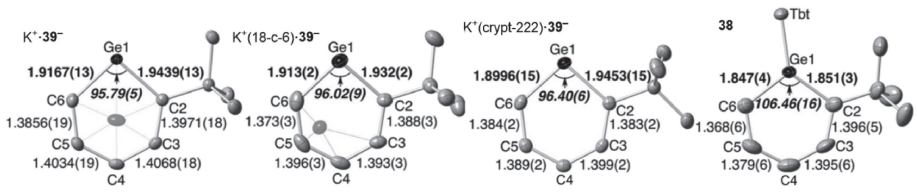

Fig. 14. Selected bond lengths [Å] and angles [°] (in italics) in K^+·**39**$^-$, K^+(18-c-6)·**39**$^-$, K^+(crypt-222)·**39**$^-$, and **38**. (*Angew. Chem. Int. Ed.* **2017**, *56*, 4588–4592)

Despite the different coordination modes, the structural parameters of these germabenzenyl potassium derivatives resembled each other. The germabenzenyl moieties adopted a planar geometry with a sum of interior angles of 720°. Within the germabenzenyl rings of K^+·**39**$^-$, K^+(18-c-6)·**39**$^-$, and K^+(crypt-222)·**39**$^-$, the C–C bond lengths were almost identical and were in the ranges of 1.3856(19)–1.4068(18), 1.373(3)–1.396(3), and 1.383(2)–1.399(2) Å, respectively. Thus, the observed values lay between typical C–C single (*ca.* 1.47 Å) and double bond (*ca.* 1.35 Å) lengths and were comparable to those of benzene (*ca.* 1.40 Å) and germabenzene **38** [1.368(6)–1.396(5) Å]. The lengths of the Ge1–C2/Ge1–C6 bonds in **39**$^-$ [1.9439(13)/1.9167(13) Å for K^+·**39**$^-$, 1.932(2)/1.913(2) Å for K^+(18-c-6)·**39**$^-$, and 1.9453(15)/1.8996(15) Å for K^+(crypt-222)·**39**$^-$] were much shorter than those of the Ge–C single bonds in carbon-substituted germylenes (>2.0 Å)[51] and comparable to those of aromatic dianionic germacyclopentadienes [1.846(9)–1.967(4) Å].[57),58] The longer lengths of Ge1–C2 compared with those of Ge1–C6 would be caused by the electron-donating character of the *tert*-butyl group. The observed planar structure of **39**$^-$, which exhibited unsaturated bonds with virtually no bond alternation, is thus in agreement with the structural criteria for aromaticity and accordingly indicates a predominant contribution from the aromatic resonance structure **39A**$^-$ (Scheme 13). Conversely, the Ge–C bond lengths were substantially longer than those of neutral germabenzene **38** [1.851(3) Å for Ge1–C2 and 1.847(4) Å for Ge1–C6]. In addition, the C6–Ge1–C2 angles [95.79(5)° in K^+·**39**$^-$, 96.02(9)° in K^+(18-c-6)·**39**$^-$, and 96.40(6)° in K^+(crypt-222)·**39**$^-$] were smaller than the angle in **38** [106.46(16)°]. These results are consistent with an increased p-character of the Ge atomic orbitals that are directed toward the ring carbon atoms upon the formation of the anion.

The refined structure of germabenzenylsodium Na^+·**39**$^-$ is presented together with that of K^+·**39**$^-$ in Fig. 15. The crystal packing of Na^+·**39**$^-$ exhibited a layer structure (Fig. 16). The germanium atom

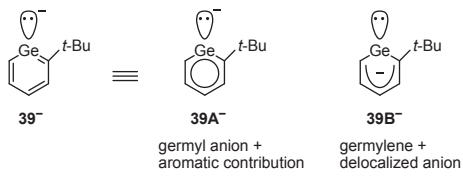

Scheme 13. Resonance structures of germabenzenyl anion **39**$^-$.

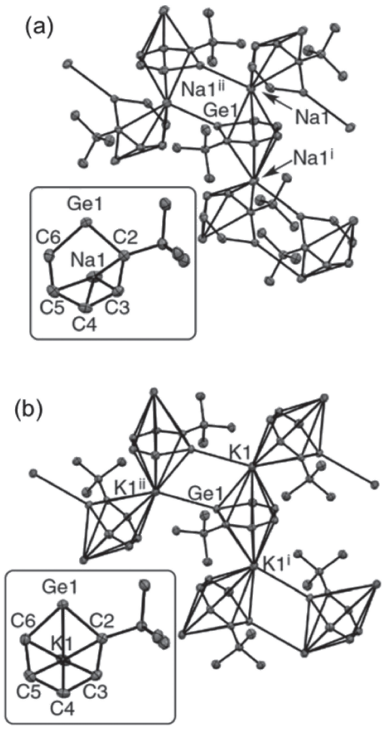

Fig. 15. Atomic displacement parameter plots and crystal packing for Na^+·**39**$^-$ (a) and K^+·**39**$^-$ (b) with thermal ellipsoids set at 50% probability. All hydrogen atoms were omitted for clarity. (*Chem. Lett.* **2018**, 47, 708–710)

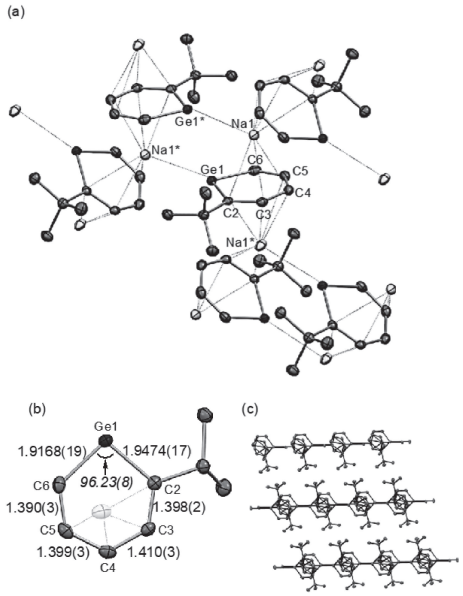

Fig. 16. Atomic displacement parameter plots for Na^+·**39**$^-$ (a) and selected bond lengths [Å] and angles [°] (in italics) in Na^+·**39**$^-$ (b) with thermal ellipsoids set at 50% probability. Crystal packing for Na^+·**39**$^-$ (c). All hydrogen atoms were omitted for clarity. (*Chem. Lett.* **2018**, 47, 708–710)

coordinated in an η^1-fashion to the sodium atom, and the germabenzenyl ring had a π-type interaction with two sodium atoms as with germabenzenylpotassium $K^+\cdot\mathbf{39}^-$. Conversely, there was a difference between the solid-state packing arrangements adopted by $K^+\cdot\mathbf{39}^-$ and $Na^+\cdot\mathbf{39}^-$. Although the potassium atom in $K^+\cdot\mathbf{39}^-$ interacted with the skeletal carbon atoms almost equally (K–C: 3.06–3.30 Å), the sodium atom in $Na^+\cdot\mathbf{39}^-$ did so unevenly (Na–C: 2.73–3.27 Å). This is most likely because the sodium atom is smaller than the potassium atom, resulting in a less effective interaction with the ring carbon atoms. Judging from this result, the interaction of lithium with the germabenzenyl ring in this mode is considered less effective than the interactions with sodium and potassium. Therefore, the properties of $Li^+\cdot\mathbf{39}^-$ are different from those of $Na^+\cdot\mathbf{39}^-$ and $K^+\cdot\mathbf{39}^-$.

As for the π-type interactions between the germabenzenyl ring and the Na atom, the Na1–C6 and Na1^i–C6 distances [3.082(2) and 3.271(2) Å] were beyond the range of those in other π-arene-sodium complexes (2.59–3.03 Å) and the Na–C distances between the sodium atom and other carbon atoms (Na1–C2, C3, C4, C5 [2.742(19)–2.963(2) Å] and Na1^i–C2, C3, C4, C5 [2.734(2)–3.107(2) Å]) were similar to those previously reported.[59] The Na1–Ge1 and Na1^i–Ge1 distances [3.2722(9) and 3.3356(8) Å] were much longer than those in germacyclopentadienyl sodium having an η^1-type interaction between the Na and Ge atoms (2.97 Å)[33a] and in germafluorenyl disodium having a π-type interaction with the sodium atom (2.93–3.06 Å).[60] These results suggest that the π-type interactions between Na1 (or Na1^i) and Ge1/C6 in $Na^+\cdot\mathbf{39}^-$ were small or negligible.

The germabenzenyl moiety in $Na^+\cdot\mathbf{39}^-$ adopted a planar geometry, with the sum of the interior angles being the expected 720°. Within the germabenzenyl ring of $Na^+\cdot\mathbf{39}^-$, the C–C bond lengths were nearly equal and were in the range of 1.390(3)–1.410(3) Å and the Ge–C bond lengths [Ge1–C2: 1.9474(17) Å; Ge1–C6: 1.9168(19) Å] were similar to the corresponding bonds of germabenzenylpotassium $K^+\cdot\mathbf{39}^-$ [Ge1–C2: 1.9439(13) Å; Ge1–C6: 1.9167(13) Å] and those of aromatic dianionic germacyclopentadienes (1.85–1.97 Å).[57] These results suggest the delocalization of π-electron over the germabenzenyl ring and the aromaticity in $Na^+\cdot\mathbf{39}^-$, similar to the case of $K^+\cdot\mathbf{39}^-$. Because the structural parameters of the germabenzenyl moieties of $Na^+\cdot\mathbf{39}^-$ and $K^+\cdot\mathbf{39}^-$ closely resembled each other, the effect of the counter ions to the germabenzenyl ring was negligible despite the difference in packing structures.

Table 1. Experimental (in THF-d_8) and theoretically calculated ^{1}H and ^{13}C chemical shifts (ppm) for $K^+\cdot\mathbf{39}^-$, $Li^+\cdot\mathbf{39}^-$, $Na^+\cdot\mathbf{39}^-$, $K^+\cdot\mathbf{39}^-$, and **38**[a]

Species	H2	H3	H4	H5	H6
$K^+\cdot\mathbf{39}^-$ (obsd.)	8.96	7.51	6.35	7.51	8.96
$Li^+\cdot\mathbf{39}^-$ (obsd.)	—	7.43	6.29	7.26	8.69
$Na^+\cdot\mathbf{39}^-$ (obsd.)	—	7.54	6.35	7.36	8.92
$K^+\cdot\mathbf{39}^-$ (obsd.)	—	7.48	6.33	7.31	8.92
39$^-$ *(calcd.)*	—	*7.60*	*6.26*	*7.49*	*9.13*
43 (obsd.)	—	7.72	6.54	7.62	7.89
43 *(calcd.)*	—	*8.17*	*6.77*	*8.08*	*7.71*
	C2	C3	C4	C5	C6
$Na^+\cdot\mathbf{39}^-$ (obsd.)	202.8	130.1	112.3	128.5	169.2
$K^+\cdot\mathbf{39}^-$ (obsd.)	203.7	130.1	112.9	128.4	171.2
$^1J(^{13}Cn,^1Hn)$	—	(137.5)	(149.8)	(142.7)	(136.9)
39$^-$ *(calcd.)*	*206.5*	*133.1*	*113.3*	*132.9*	*179.1*
43 (obsd.)	163.0	138.9	114.5	138.0	138.4
$^1J(^{13}Cn,^1Hn)$	—	(159.0)	(156.4)	(146.3)	(152.3)
43 *(calcd.)*	*170.0*	*144.3*	*117.8*	*143.9*	*145.9*

[a] Theoretical values calculated at the B3LYP/6-311G(2df,2p)//B3LYP/6-31G(d,p) level of theory. $^1J(^{13}C,^1Hn)$ values (Hz) are in parentheses.

3.4. NMR spectroscopic analysis. The ^{1}H and ^{13}C NMR chemical shifts for $Li^+\cdot\mathbf{39}^-$, $Na^+\cdot\mathbf{39}^-$, $K^+\cdot\mathbf{39}^-$, and neutral germabenzene **38** in THF-d_8 are summarized in Table 1, together with the theoretical values for the aforementioned optimized structure of $\mathbf{39}^-$. The NMR chemical shifts for the proton and carbon atoms in the ring of $\mathbf{39}^-$ were characteristically shifted downfield, and the experimentally observed resonances were consistent with the calculated ones. Moreover, the addition of an equimolar amount of crypt-222 to the THF-d_8 solution of $\mathbf{39}^-$ induced merely negligible changes to the ^{1}H NMR chemical shifts ($\Delta\delta \approx 0.2$ ppm). These results suggest the presence of a separated ion pair in THF, consisting of a fully solvated potassium cation $[K(thf)_n]^+$ and isolated anion $\mathbf{39}^-$. Conversely, a relatively large difference in the chemical shifts of H6 was observed between the Li and Na/K systems. This is probably due to the weak interaction of Li^+ with the germabenzenyl moiety and/or the contamination of the byproducts.

Although the chemical resonances for H3–H5 in $K^+\cdot\mathbf{39}^-$ were shifted slightly upfield compared with those of neutral germabenzene **43** in THF-d_8, the chemical resonance for H6 (8.92 ppm) was drastically downfield-shifted relative to that of **43** (7.89 ppm). The ^{13}C NMR spectrum of $K^+\cdot\mathbf{39}^-$ exhibited downfield-shifted resonances for the carbon atoms (C2 and

C6) and upfield-shifted resonances for C3–C5 relative to the corresponding resonances in **43**. The downfield shifts for the α carbon atoms and the associated protons, as well as the upfield shifts for other atoms, were identical to the changes observed in the phenyllithium/benzene (^{1}H NMR in THF-d_8: $o/m/p = \delta$ 7.98/6.93/6.83 *vs.* 7.31; ^{13}C NMR in THF-d_8: $o/m/p = \delta$ 144.2/125.0/123.3 *vs.* 128.8)[61] and pyridine/pyridinium (^{13}C NMR in D_2O: $o/m/p = \delta$ 148/124/137 *vs.* 141/128/147)[62] systems. The downfield shifts of the α carbon atoms may be explained by the enhanced paramagnetic electron circulation, resulting from the perpendicular orientation of the lone pair on the germanium atom with respect to the π* orbitals of the ring. Although the $^1J(^{13}C,^1H)$ values for **43** were observed in a typical sp^2 region [$^1J(^{13}C,^1H)$ for benzene = 158 Hz)], those for $K^+\cdot\mathbf{39}^-$, particularly ^1J(C3,H3) and ^1J(C6,H6), were quite smaller than those of other typical sp^2 compounds, in addition to **38**, suggesting the increased p-character of C atomic orbitals that were directed toward protons.

The ^{7}Li NMR signal attributed to $Li^+\cdot\mathbf{39}^-$ was observed at +1.60 ppm. The signal was observed at a characteristically downfield position compared with the typical delocalized lithium cyclopentadienide derivatives, which exhibited highly upfield-shifted signals due to their aromatic ring current [−8.37 ppm for C_5H_5Li,[63] −7.51 ppm for $(HMe_2Si)_5C_5Li$,[64] and −5.63 ppm (η^5-Li) for $Et_4C_4GeLi_2$[58c]]. It was comparable to those of alkyllithiums, aryllithiums,[65] η^1-germyllithiums (−0.93 ppm),[66] and stannyllithium (ranging from −0.74 to +0.95 ppm).[67] This result, at least, suggests that $Li^+\cdot\mathbf{39}^-$ has no π-type interaction with Li^+ in THF solution, as observed in the crystal structure of the Na and K derivatives.

3.5. UV–vis spectroscopic studies and theoretical calculations. The UV–vis spectra of $Na^+\cdot\mathbf{39}^-$ and $K^+\cdot\mathbf{39}^-$ in THF (Fig. 17) exhibited an absorption at 324 nm ($\varepsilon = 8.0 \times 10^3$) for $Na^+\cdot\mathbf{39}^-$ and 329 nm ($\varepsilon = 5.2 \times 10^3$) for $K^+\cdot\mathbf{39}^-$, together with a shoulder at ∼360 nm ($\varepsilon = 1.9 \times 10^3$) for $Na^+\cdot\mathbf{39}^-$ and ∼358 nm ($\varepsilon = 2.0 \times 10^3$) for $K^+\cdot\mathbf{39}^-$, which slightly differ from each other. Conversely, the simulated UV–vis absorption spectrum of $\mathbf{39}^-$ derived from time-dependent (TD)-DFT calculations was still in good agreement with the observed spectrum. The absorption shoulder at ∼360 nm could be assigned to the n-π* transition from the HOMO-1 to the LUMO. The absorption at 324 and 329 nm consists mainly of π–π* transitions from the HOMO (Fig. 18).

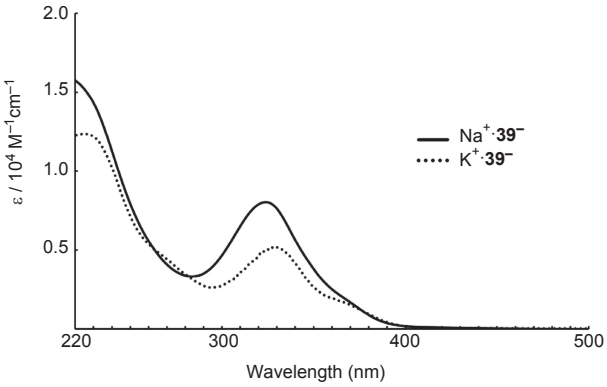

Fig. 17. UV–vis spectra of $Na^+\cdot\mathbf{39}^-$ and $K^+\cdot\mathbf{39}^-$ in THF. (*Chem. Lett.* **2018**, 47, 708–710)

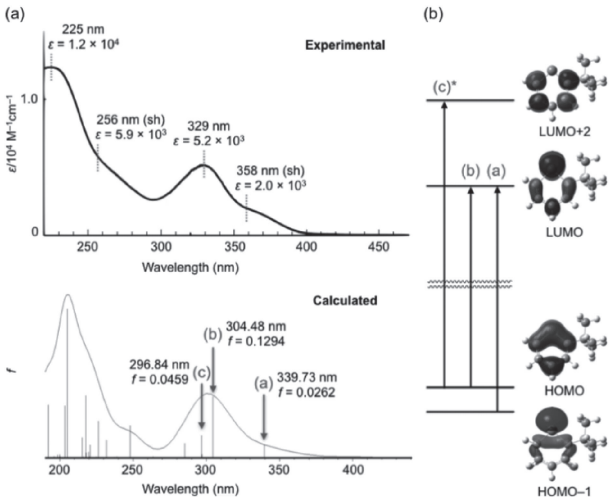

Fig. 18. (a) Top: observed UV–vis absorption spectrum for $K^+\cdot\mathbf{39}^-$ in THF at 298 K. Bottom: simulated UV–vis absorption spectrum for $\mathbf{39}^-$, whereby calculated oscillator strengths are shown as gray vertical lines. (b) Electronic transitions corresponding to the absorptions **a**–**c**. *: Absorption **c** contained contributions from several transitions. (*Angew. Chem. Int. Ed.* **2017**, *56*, 4588–4592)

NMR and UV–vis spectroscopic analyses, along with the theoretical calculations, may suggest an indispensable and partial interaction between the germabenzenyl ring and counter cations, though compounds $M^+\cdot\mathbf{39}^-$ in THF solution can be considered separated ion pairs, that is, $[M(thf)_n]^+$ and $\mathbf{39}^-$, dominantly. The molecular orbitals (MOs) and the associated energy levels for benzene, phenyl anion **43**, germabenzene **44**, and the parent germabenzenyl anion ($[GeC_5H_5]^-$) $\mathbf{37}^-$ are summarized in Fig. 19.

The corresponding results for $\mathbf{39}^-$ exhibited a trend similar to that of $\mathbf{37}^-$ (Fig. 20). The frontier orbitals situated in $\mathbf{37}^-$ were similar to those of the

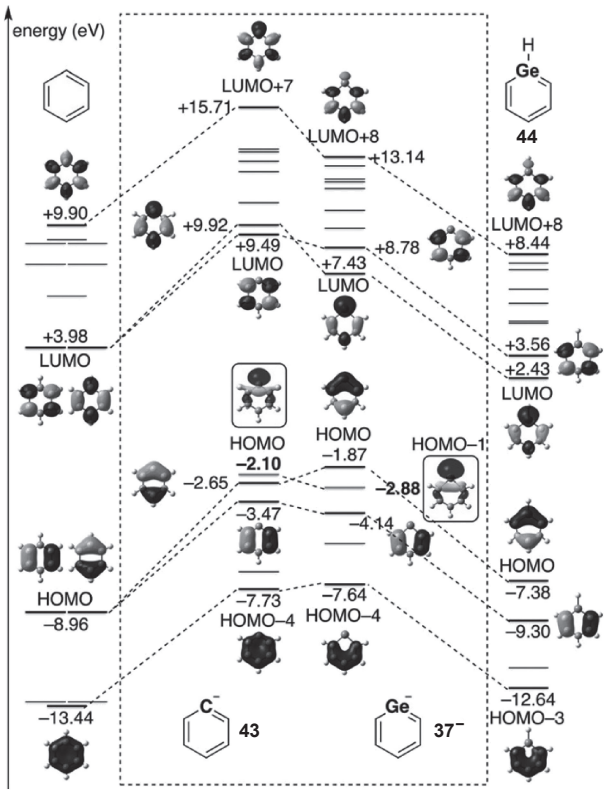

Fig. 19. Molecular orbitals for benzene, phenyl anion **43**, germabenzene **44**, and germabenzenyl anion **37**$^-$ calculated at the HF/6-31G(d,p)//B3LYP/6-31G(d,p) level of theory (isovalues = 0.04). (*Angew. Chem. Int. Ed.* **2017**, *56*, 4588–4592)

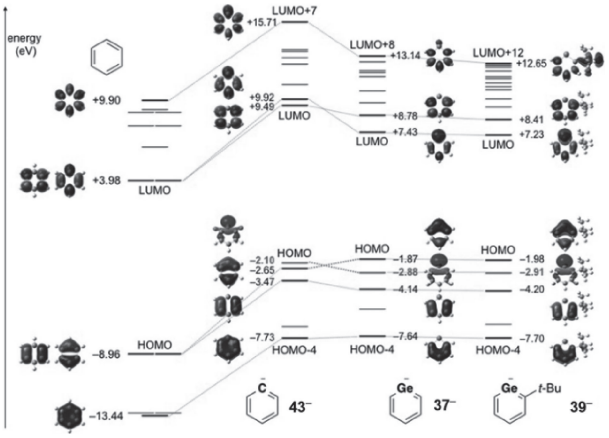

Fig. 20. Molecular orbitals for benzene, phenyl anion **43**, and the germabenzenyl anions **37**$^-$ and **39**$^-$ calculated at the HF/6-31G(d,p)//B3LYP/6-31G(d,p) level of theory (isovalues = 0.04). (*Angew. Chem. Int. Ed.* **2017**, *56*, 4588–4592)

phenyl anion. Similar to the case of benzene and phenyl anion, six π-type MOs were found and three of these were filled with six π-electrons. The most

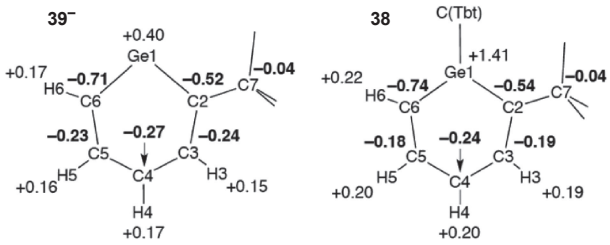

Fig. 21. NPA charges for **39**$^-$ and **38** calculated at the B3LYP/6-311G(2df,2p) level of theory. (*Angew. Chem. Int. Ed.* **2017**, *56*, 4588–4592)

notable feature was observed in the nonbonding orbitals, which was the HOMO (−2.10 eV) in the phenyl anion and the HOMO-1 (−2.88 eV) in **37**$^-$. The lower orbital level in **37**$^-$ should be due to the inert 4s orbital character of the germanium atom, which was caused by the preferred $(ns)^2(np)^2$ valence electron configuration of heavy Group 14 elements. The energy level of the LUMO of **37**$^-$ (+7.43 eV), which involved a p-orbital of germanium, was lower relative to the corresponding orbital in the phenyl anion, that is, the LUMO+1 (+9.92 eV). In contrast to the HOMO-4 of the phenyl anion, that of **37**$^-$ included no Ge orbitals but predominantly delocalized on the C_5 moiety, suggesting less effective conjugation between the 4p AO (Ge) and the 2p AO (C) relative to the 2p(C^-)–2p(CH) conjugation in the phenyl anion.

The natural population analysis (NPA) charges for **39**$^-$ and **38** showed virtually identical charge contributions from each atom of the C_5 moiety, and the germanium atom represented the only difference between **39**$^-$ and **38** (Fig. 21).

This result suggests a small diamagnetic and large paramagnetic contribution to the differences in the ^{1}H and ^{13}C chemical shifts between K^+·**39**$^-$ and **38**. The NPA and MO analyses suggest the electronic structure of **39**$^-$ as the predominant contributions from the aromatic canonical resonance structure **39A**$^-$, along with the insufficient overlap between the p-orbitals of the Ge and C atoms representing **39B**$^-$ to some extent. The remarkable stability of **39**$^-$ as a monomeric structure could be most likely interpreted in terms of charge repulsion as a result of its anionic charge delocalized on the GeC_5 ring. In addition, a germabenzenyl anion would intrinsically exhibit considerable stability due to the stable oxidation state of Ge^{II} in **39**$^-$, relative to that of neutral germabenzene with a Ge^{IV} oxidation state.

3.6. Summary for germabenzenyl anions. We have synthesized and isolated K^+·**39**$^-$, a germa-

nium analog of phenyl potassium, which exists as a monomer both in solution and in the solid state. Its ambident character, exhibiting both aromatic and germylene features, was confirmed both spectroscopically and structurally and was supported by the results of the theoretical calculations.

Furthermore, germabenzenyllithium $Li^+ \cdot \mathbf{39}^-$ and -sodium $Na^+ \cdot \mathbf{39}^-$ were obtained by the reactions of 1-Tbt-2-*tert*-butylgermabenzene **38** with sodium and lithium naphthalenides. $Na^+ \cdot \mathbf{39}^-$ was structurally and spectroscopically characterized. Although the packing structure of $Na^+ \cdot \mathbf{39}^-$ differed from that of $K^+ \cdot \mathbf{39}^-$, the results of the NMR and UV–vis spectroscopic analyses and the structural parameters of $Na^+ \cdot \mathbf{39}^-$ were almost similar to those of $K^+ \cdot \mathbf{39}^-$. The counter ion had little influence on the germabenzenyl ring.

4. Stannabenzenyl anion: A tin analog of a phenyl anion

4.1. Heavier metallabenzenyl anions. As described in the previous section, we succeeded in the synthesis and isolation of germabenzenyl anions $\mathbf{37}^-$ and $\mathbf{39}^-$ by the reaction of neutral germabenzenes bearing a bulky aryl group with several reducing agents. Its ambident character, exhibiting aromatic **A** and germylene **B** features, was confirmed both spectroscopically and structurally and was supported by the results of the theoretical calculations. Conversely, it is known that heavier Group 14 atoms (Si, Ge, Sn, and Pb) have a low ability to form hybrid orbitals and they therefore prefer the $(ns)^2(np)^2$ valence electron configurations in their divalent species.[68] Because two electrons remain as a singlet pair in the ns orbital, the ground state of H_2M: (M = Si, Ge, Sn, and Pb) is a singlet, unlike the case of H_2C:, where the ground state is a triplet.[69] Furthermore, the relative stabilities of the singlet species of R_2M: (M = C, Si, Ge, Sn, and Pb; R = alkyl or aryl) are estimated to increase as the element row descends, C < Si < Ge < Sn < Pb.[70] It follows therefore that one can expect that the tin and lead analogs of a phenyl anion should exhibit high metallylene and low aromatic features compared with the corresponding germabenzenyl anion. Then, on the basis of this situation, we next challenged the synthesis of a stable stannabenzenyl anion using a synthetic method similar to that of germabenzenyl anions $\mathbf{37}^-$ and $\mathbf{39}^-$.

4.2. Generation of neutral stannabenzenes. To synthesize a stannabenzenyl anion using the same method as that in the case of germabenzenyl anions $\mathbf{37}^-$ and $\mathbf{39}^-$, we need to synthesize a kinetically stabilized, neutral stannabenzene bearing a bulky aryl group. However, the attempts to generate stannabenzenes **45** having a Tbt or Bbt group on the tin atom resulted in the almost quantitative formation of [4 + 2]-dimer **46** of stannabenzene **45** (Scheme 14).[71] As estimated by DFT calculations, the extremely high reactivity of a stannabenzene marks a sharp contrast with the considerably high thermal stability of Tbt-substituted sila-[25] and germabenzenes[26] (stable at 100 °C in C_6D_6), probably due to the smaller HOMO–LUMO gap of **45** compared with its lighter congeners. Then, to synthesize and isolate a stable stannabenzene, an additional substituent (*tert*-butyl) was introduced on the carbon atom adjacent to the tin atom. The synthesis of stannabenzenes **46** was performed by the dehydrobromination of the corresponding bromostannane precursor with lithium diisopropylamide (Scheme 14).

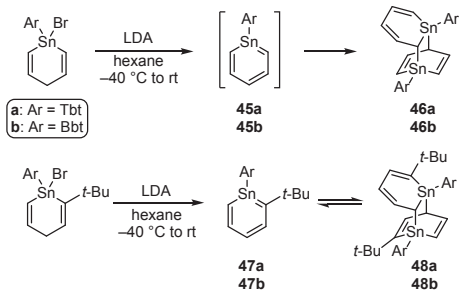

Scheme 14. Generation of stannabenzenes **45** and **47**.

In the case using a Tbt-substituted precursor, contrary to our expectation, only the formation of head-to-tail [4 + 2] dimers **46a** was observed at room temperature. In the case using the Bbt-substituted one, conversely, the formation of monomeric stannabenzene **47b** together with that of the corresponding dimer **48b** was strongly suggested, judging from the ^1H and ^{119}Sn NMR spectra. The ^1H NMR spectra at various temperatures showed the changes of the **47**:**48** ratio, and that in the case of the Bbt-substituted system at 80 °C in C_6D_6 indicated the almost exclusive existence of **47b**. The ^1H NMR measurement at room temperature after heating reproduced the initial **47b**:**48b** ratio without any decomposition, indicating the existence of an equilibrium between **47b** and **48b**. This equilibrium was also supported by the UV–vis spectra at various temperatures, showing the isosbestic point. Similarly, the equilibrium between Tbt-substituted derivatives **47a** and **48a** was suggested by the results of the

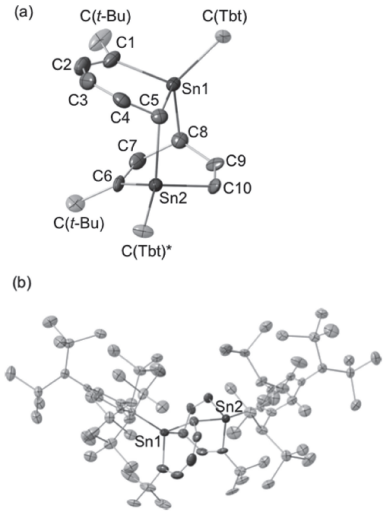

Fig. 22. Thermal ellipsoid plot (50% probability) of the stannabenzene dimer [**48a**·benzene]; the core (a) and whole (b) structures. Hydrogen atoms, the benzene molecule, and the disordered part were omitted for clarity. (*Dalton Trans.* **2008**, *47*, 14436–14444)

^{1}H NMR measurement at various temperatures, but dimer **48a** was still observed even at 80 °C in C_6D_6.

The structures of dimers **48a** and **48b** were reasonably established by the measurement of 1D (^{1}H, ^{13}C, and ^{119}Sn) NMR and HH-COSY spectra and NOE experiments. Meanwhile, single crystals of **48a** were obtained by recrystallization from its benzene solution, and the molecular structure of [**48a**·benzene] was confirmed by crystallographic analysis, as shown in Fig. 22. Severe disorders due to pseudosymmetry were observed on the core $(SnC_5)_2$ moiety, and thus, the structural parameters cannot be discussed in detail.

The ^{119}Sn NMR signals of **48b** showed two sharp signals at −220 and −177 ppm, indicating the formation of a single isomer. Those of **48a** showed two signals at approximately −220 ppm and four signals at approximately −173 ppm at room temperature, suggesting the existence of isomers derived from the several configurations of the $CH(SiMe_3)_2$ moieties on the Tbt group due to steric congestion. This type of rotational isomers was suggested in some systems using the Tbt group,[72] and the ^{119}Sn NMR signals of **48a** broadened and coalesced at 70 °C (one broadened signal at −220 ppm and two signals at approximately −173 ppm).

4.3. Synthesis of stannabenzenylpotassium.[73] Because our attempts at synthesizing a stable stannabenzene using a bulky substituent only on the tin atom were unsuccessful, we introduced an additional substituent (*tert*-butyl) on the carbon atom adjacent to the tin atom. Although this approach led to an equilibrated mixture of the corresponding stannabenzene **47** and its dimer **48** in solution, the equilibrium mixture would still be a suitable precursor to gain the stannabenzenyl anion.

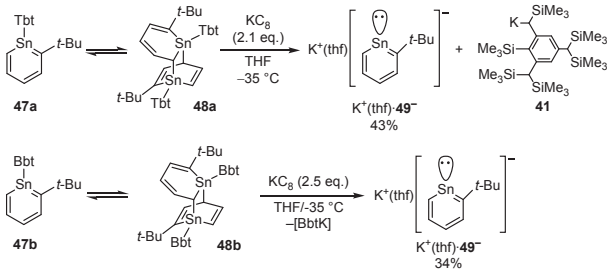

Scheme 15. Synthesis of stannabenzenylpotassium K$^+$(thf)·**49**$^-$.

The reaction of the mixture of **47a** and **48a** (Ar = Tbt) with 2.1 equivalents of potassium graphite in THF successfully resulted in the formation of stannabenzenylpotassium K$^+$(thf)·**49**$^-$ in 43% yield (Scheme 15). The Tbt moiety was extruded as benzylpotassium **41** mainly and removed by washing of the reaction mixture with *n*-hexane and benzene. Compound K$^+$(thf)·**49**$^-$ was insoluble in *n*-hexane or benzene and soluble in THF, the extraction of the remaining materials mentioned above with THF afforded pure K$^+$(thf)·**49**$^-$ as a purple solid, and the THF solution of K$^+$(thf)·**49**$^-$ exhibited a yellow color. K$^+$(thf)·**49**$^-$ is highly moisture-sensitive both in the solid state and in solution. Although the measurement of the UV–vis spectra of K$^+$(thf)·**49**$^-$ in the solid state was unsuccessful because of its instability, the reason for the color difference between the solid and solution states was considered to be the expansion of the MOs to the neighboring SnC_5 moiety through the Sn···Sn moiety in the solid state as suggested by the TD-DFT calculations (for the details, described later). As in the case of the Tbt system, treatment of an equilibrated mixture of **47b** and **48b** (Ar = Bbt) with 2.5 equivalents of potassium graphite in THF at −35 °C afforded stannabenzenylpotassium K$^+$(thf)·**49**$^-$ in 34% yield (Scheme 15).

4.4. NMR spectroscopic analysis and NICS values.[8),74),75] The ^{1}H, ^{13}C, and ^{119}Sn NMR chemical shifts of stannabenzenylpotassium K$^+$(thf)·**49**$^-$ in THF-d_8 are listed in Table 2, along with the observed values for the germanium analog, K$^+$·**39**$^-$, and the calculated values for the free anion **49**$^-$ obtained by the GIAO method on the B3LYP/[4333111/

Table 2. Experimental (in THF-d_8) ^{1}H and ^{13}C NMR chemical shifts (ppm) for K^+(thf)·**49**$^-$ and K^+·**39**$^-$ and theoretically calculated values for **49**$^-$[a]

Species	Sn1	H3	H4	H5	H6
K^+(thf)·**49**$^-$ (obsd.)	700.8	7.84	6.39	7.77	9.91
49$^-$ *(calcd.)*	*492.8*	*7.87*	*6.15*	*7.77*	*10.02*
K^+·**39**$^-$ (obsd.)	—	7.48	6.33	7.31	8.92
	C2	C3	C4	C5	C6
K^+(thf)·**49**$^-$ (obsd.)	226.0	133.2	113.6	130.8	189.6
49$^-$ *(calcd.)*	*231.3*	*136.6*	*112.5*	*136.0*	*195.3*
K^+·**39**$^-$ (obsd.)	203.7	130.1	112.9	128.4	171.2

[a] Theoretical values calculated at the B3LYP/[4333111/433111/4311][Sn],6-311G(2df,2p)[CH]//B3LYP/Lanl2DZ[Sn],6-31G(d,p)[CH] level of theory.

433111/4311][Sn],6-311G(2df,2p)[CH]//B3LYP/Lanl2DZ[Sn],6-31G(d,p)[CH] level of theory. All ^{1}H and ^{13}C NMR chemical shifts assigned to the stannabenzenyl ring of K^+(thf)·**49**$^-$ were observed in the characteristic low-field region. The observed values were in good agreement with the calculated ones for free anion **49**$^-$, suggesting the presence of a separated ion pair in THF, consisting of a fully solvated cation, [K^+(thf)$_n$], and isolated anion **49**$^-$. The signals assignable to those of H6 and C2/6 were significantly shifted to a lower field (9.91 and 226.0/189.6 ppm, respectively) as compared with those of the corresponding atoms on K^+·**39**$^-$ (8.92 and 203.7/171.2 ppm). This trend of the lower-field shift with the increase in atomic number was observed similarly in the Tbt-substituted neutral heavy benzenes (sila-,[25] germa-,[26] and stannabenzenes) and heavy pyridines (phospa-, arsa-, stiba-, and bismabenzenes).[76),77] It was explained in terms of the magnetic anisotropy of heavier elements, which was expected to increase with atomic number.

The ^{119}Sn NMR spectrum of K^+(thf)·**49**$^-$ displayed a sharp resonance at +702 ppm. This shift was located at the middle of the ranges of the reported tin-containing aromatic compounds [stannole dianions: −27.8 to +472.6 ppm[46c),78]; stannabenzenes **47**: +275.5 (Ar = Tbt) and +271.4 (Ar = Bbt) ppm; and 2-Tbt-2-stannanaphthalene: +270 ppm][79] and stannylenes (∼2000 ppm),[49] suggesting the contribution of a resonance form with stannylene character **49B**$^-$ in **49**$^-$ (Scheme 16). Although the difference between the observed and calculated values for the tin atom was very large to ignore, it can be said to be reproduced well, taking the large chemical shift range of ^{119}Sn NMR (∼6000 ppm) into account.

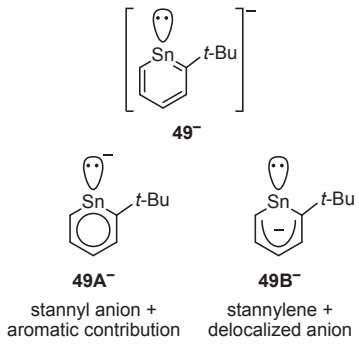

Scheme 16. Resonance structures for stannabenzenyl anion **49**$^-$.

We conducted the NICS analysis of **49**$^-$ at the same level of theory as mentioned above, showing NICS(0) and NICS(1) values of −5.08 and −7.26, respectively.[74] Although these absolute values were smaller than the calculated NICS(0) and NICS(1) values for phenyl anion **43**$^-$ (−6.97 and −10.56, respectively) and **39**$^-$ (−5.48 and −8.10, respectively), they still suggest the aromatic character of **49**$^-$. The NICS$_{zz}$(r) values[75] [r is the distance (Å) from the geometrical center of the ring along the z-axis, which is oriented perpendicular to the plane of the ring] were calculated to evaluate the distance dependency of the NICS calculations. Figure 23 shows the results for benzene, phenyl anion, germabenzene **44**, germabenzenyl anion **39**$^-$, stannabenzene **50**, and stannabenzenyl anion **49**$^-$. The NICS$_{zz}$ profiles for the phenyl anion, **39**$^-$, and **49**$^-$ resembled those of the corresponding neutral systems. The highest absolute NICS values were obtained at ∼1.0 Å (benzene/phenyl anion), ∼1.1 Å (**44**), and ∼1.2 Å (**49**$^-$, **39**$^-$, and **50**) above the ring centers. Those for the germanium and tin systems were

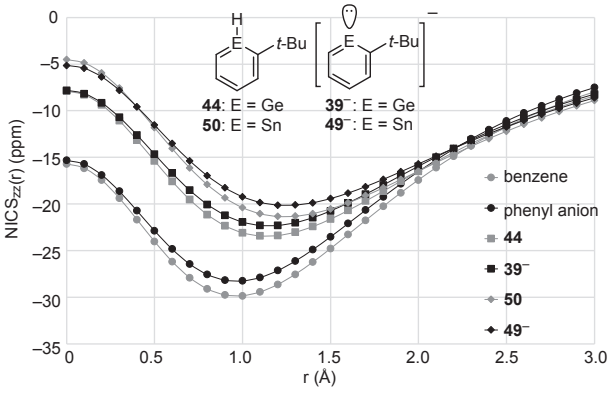

Fig. 23. NICS$_{zz}$(r) profiles for **49**$^-$ and the related compounds. (*Chem. Eur. J.* **2018**, *24*, 17039–17045)

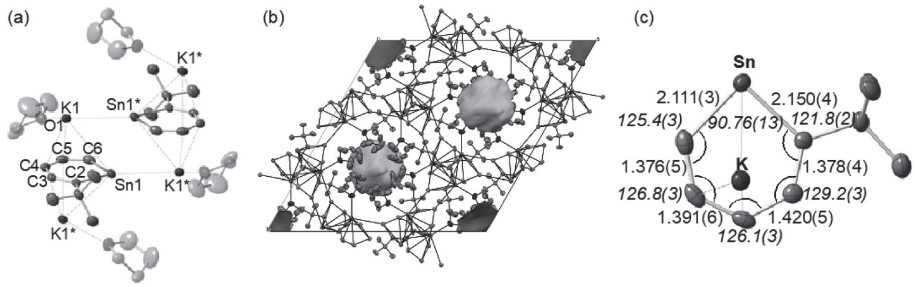

Fig. 24. (a) Atomic displacement parameter plots for $K^+(thf)\cdot\mathbf{49}^-$ at 50% probability. (b) Crystal packing in a unit cell; the gray area shows the void removed by SQUEEZE, which may contain a THF molecule. (c) Selected bond lengths (Å) and angles (°) in $K^+(thf)\cdot\mathbf{49}^-$. (*Chem. Eur. J.* **2018**, *24*, 17039–17045)

slightly away from the central ring as compared with the case of carbon, reflecting the larger π-orbitals of Ge and Sn relative to C. Even though the highest absolute $NICS_{zz}(r)$ value for $\mathbf{49}^-$ (−20.1 ppm) was smaller than the values for the others, it still suggests considerable aromaticity for $\mathbf{49}^-$.

4.5. X-Ray diffraction studies of the stannabenzenyl anion. Purple X-ray quality crystals of $K^+(thf)\cdot\mathbf{49}^-$ were obtained from a cold (−35 °C) THF/*n*-hexane mixture. Although three potassium atoms (crystallographically equal) were situated close to one stannabenzenyl ring similarly to the case of $K^+\cdot\mathbf{39}^-$, they were coordinated by a THF molecule (Fig. 24a). In contrast to the layer packing of $K^+\cdot\mathbf{39}^-$, the packing of $K^+(thf)\cdot\mathbf{49}^-$ showed the three-dimensional infinite structure with the tubular spaces filled by THF molecules (Fig. 24b).

The structural analysis (Fig. 24c) revealed the planarity of the stannabenzenyl ring, in which the sum of the bond angles around the central tin atom and that of the interior bond angles of the stannabenzenyl ring were 359° and 720°, respectively. The lengths of the four C–C bonds of the stannabenzenyl ring [1.376(5)–1.420(5) Å] were also roughly intermediate between those of the C–C double (1.34 Å) and single [1.47 Å (sp^2–sp^2)] bonds. The lengths of the Sn–C2/Sn–C6 bonds in $K^+(thf)\cdot\mathbf{49}^-$ [2.150(4)/2.111(3) Å] were shorter than those of the aromatic stannole dianions (2.17–2.20 Å). These results suggest that the π-electrons in the stannabenzenyl ring system of $K^+(thf)\cdot\mathbf{49}^-$ were delocalized to show a predominant contribution of aromatic character $\mathbf{49A}^-$ similar to the case of its germanium analog $K^+\cdot\mathbf{39}^-$.

However, the degree of bond alternation of $K^+(thf)\cdot\mathbf{49}^-$ was much larger than that of $K^+\cdot\mathbf{39}^-$ and the lengths of C2–C3 [1.378(4) Å] and C5–C6 [1.376(5) Å] were particularly short, suggesting the

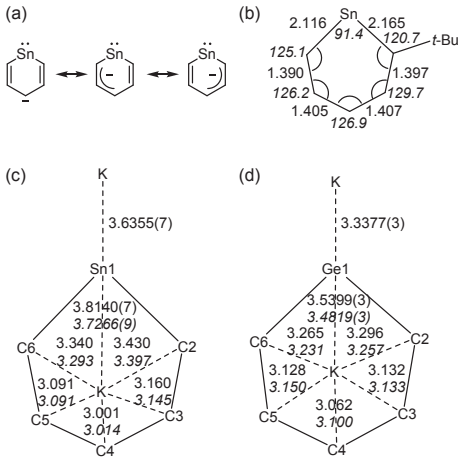

Fig. 25. (a) Major resonance structures of $K^+(thf)\cdot\mathbf{49}^-$ in the solid state. (b) Selected bond lengths (Å) and angles (°) in the optimized structure of free $\mathbf{49}^-$. (c), (d) Distances (Å) between the potassium atoms and skeletal elements of $K^+(thf)\cdot\mathbf{49}^-$ and $K^+\cdot\mathbf{39}^-$. Plain and italic values correspond to the distances with the potassium atoms above and below the paper, respectively. Standard deviations for K–C distances were omitted. (*Chem. Eur. J.* **2018**, *24*, 17039–17045)

large contribution of the resonance structures in Fig. 25a. The optimized structures of the free anion $\mathbf{49}^-$ on B3LYP/Lanl2DZ[Sn],6-31G(d,p)[CH] (Fig. 25b), reproducing the properties in solution [NMR and UV–vis spectra (as described later)] well, and on other basis sets were different from the observed one, in contrast to the good agreement between the observed and calculated structures in the germanium case. This is because the potassium atom of $K^+(thf)\cdot\mathbf{49}^-$ in the solid state affected the C_5 moiety more strongly than that of $K^+\cdot\mathbf{39}^-$. Actually, the distances between the potassium and skeletal atoms of EC_5 of $K^+(thf)\cdot\mathbf{49}^-$ were very different from those of $K^+\cdot\mathbf{39}^-$, and the position of

the potassium atom in $K^+(thf)\cdot\mathbf{49}^-$ approached closely to the C4–C5 moiety [*e.g.*, K–C4: 3.001/3.014 Å in $K^+(thf)\cdot\mathbf{49}^-$ *vs.* 3.062/3.100 Å in $K^+\cdot\mathbf{39}^-$] (Figs. 25c, d). Although we tried structural optimization on various models, including potassium atoms and/or THF molecules with various methods/basis sets, the bond shortening of C2–C3 and C5–C6 could not be reproduced. This is probably because a packing force affected the structural parameters.

Conversely, the Sn–C bond lengths [2.150(4)/2.111(3) Å] were substantially longer than those of neutral 2-stannanaphthalene [2-Tbt-2-stannanaphthalene, 2.081(6) and 2.029(6) Å].[79] In addition, the C6–Sn–C2 angle in $K^+(thf)\cdot\mathbf{49}^-$ [90.76(13)°] was smaller than the angles in 2-stannanaphthalene [100.0(3)°] and $K^+\cdot\mathbf{39}^-$ [95.78(5)°] and approached 90°.

4.6. Theoretical calculations. From the structural aspects, we can conclude that the contribution of metallylene form $\mathbf{49B}^-$ in $K^+(thf)\cdot\mathbf{49}^-$ becomes larger than that of $\mathbf{39B}^-$ in $K^+\cdot\mathbf{39}^-$, which is in agreement with its decrease in aromaticity. This was supported by the results of the natural bond orbital (NBO) analysis of $\mathbf{49}^-$,[80] showing that a lone pair on the tin atom had a higher s-character ($sp^{0.32}$) than that on the germanium atom of $\mathbf{39}^-$ ($sp^{0.42}$) and that the AOs (Sn) on the Sn–C σ bonds had a higher p-character ($sp^{6.30}$ and $sp^{7.10}$) than that of the AOs (Ge) on the Ge–C bonds of $\mathbf{39}^-$ ($sp^{5.20}$ and $sp^{5.47}$), as shown in Fig. 25.

To elucidate the electronic structure of stannabenzenyl anion $\mathbf{49}^-$, the frontier orbitals for the parent stannabenzenyl and germabenzenyl anions ($\mathbf{51}^-$ and $\mathbf{37}^-$) and phenyl anion were calculated at the HF/Lanl2DZ[Sn],6-31G(d,p)[CHGe]//B3LYP/Lanl2DZ[Sn],6-31G(d,p)[CHGe] levels of theory, as shown in Fig. 26. Because the models with the *tert*-butyl group showed negligible differences, the results for those without the *tert*-butyl group were shown. Similar to the cases of phenyl anion and $\mathbf{37}^-$, six π-type MOs were found and three of these were filled with six π-electrons. The most characteristic feature of heavy phenyl anions as compared with phenyl anions was the switch of the HOMO and HOMO–1. The HOMO of $\mathbf{51}^-$, which corresponded to the π orbital, was much more destabilized than that of $\mathbf{37}^-$. Conversely, the energy level of its HOMO–1, corresponding to the nonbonding orbital, was almost the same as that of $\mathbf{37}^-$. The LUMO of $\mathbf{51}^-$, involving the p-orbital of tin, was drastically (3.4 eV more) stabilized as compared with the corresponding orbital of phenyl anions (LUMO+1).

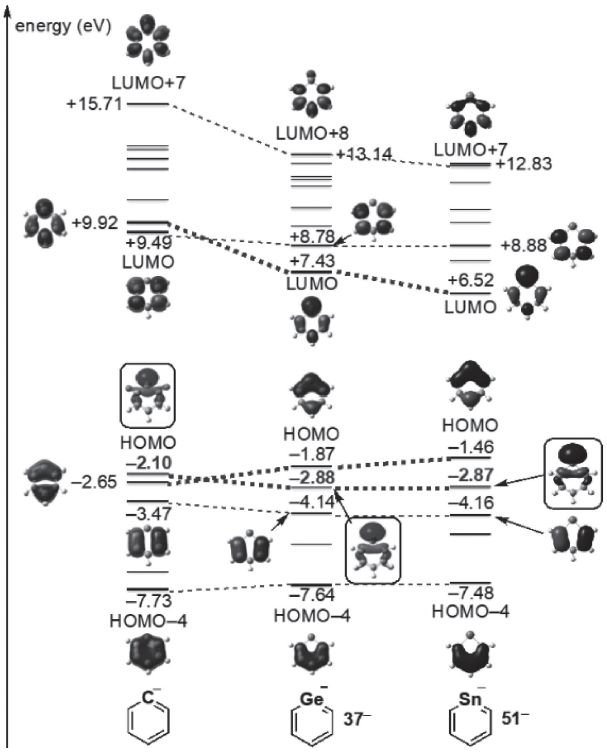

Fig. 26. Molecular orbitals for the phenyl anion, germabenzenyl anion $\mathbf{37}^-$, and stannabenzenyl anion $\mathbf{51}^-$ calculated at the HF/Lanl2DZ[Sn],6-31G(d,p)[CHGe]//B3LYP/Lanl2DZ[Sn],6-31G(d,p)[CHGe] level of theory (isovalues = 0.04). (*Chem. Eur. J.* **2018**, *24*, 17039–17045)

Other orbitals of $\mathbf{51}^-$ and $\mathbf{37}^-$ not involving a heavy element showed almost the same levels.

As described previously, compound $K^+(thf)\cdot\mathbf{49}^-$ showed a purple color in the solid state and a yellow color in solution. This drastic change was in sharp contrast to the germanium case $K^+\cdot\mathbf{39}^-$ (yellow/orange solid and yellow solution in THF). To investigate this color difference, TD-DFT calculations using the part of the infinite structure of $K^+(thf)\cdot\mathbf{49}^-$ determined by the X-ray crystallographic analysis were performed. As a result, the model with a $[K(thf)\cdot\mathbf{49}_3]^{2-}$ structure (Fig. 27), reproducing the coordination around the potassium atom, could explain the observed phenomena. As described in Section 4.7, the UV–vis spectra of $K^+(thf)\cdot\mathbf{49}^-$ in THF were in good agreement with the simulated spectrum using free anion $\mathbf{49}^-$.

The structural optimization of $[K(thf)\cdot\mathbf{49}_3]^{2-}$ was performed using the atom coordinates determined by X-ray crystallographic analysis with Opt= ReadFreeze (with "noatoms atoms=H") keyword to fix the geometry of all atoms, except for H atoms at

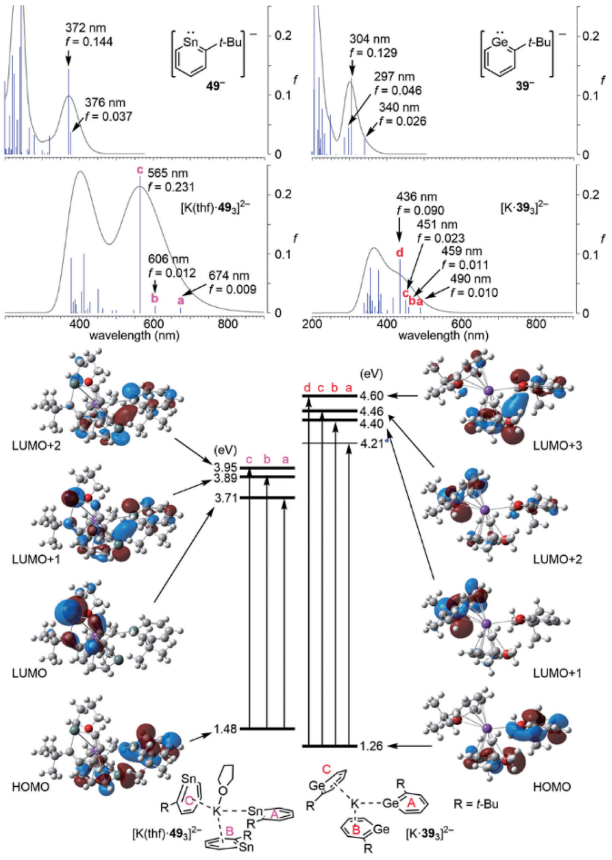

Fig. 27. (Top) Simulated UV–vis spectra for **49**$^-$, **39**$^-$, $[K(thf)\cdot\mathbf{49}_3]^{2-}$, and $[K\cdot\mathbf{39}_3]^{2-}$ derived from TD-DFT calculations at the B3LYP/4333111/433111/4311[Sn],6-311G(2df,2p)[others]//B3LYP/Lanl2DZ[Sn],6-31G(d,p)[others] level of theory. (Bottom) Electronic transitions corresponding to the absorptions **a**–**c** and **a**–**d**. LUMO of $[K\cdot\mathbf{43}_3]^{2-}$ was widely spread around the periphery of the molecule. (*Chem. Eur. J.* **2018**, *24*, 17039–17045)

the B3LYP/Lanl2DZ[Sn],6-31G(d,p)[others] level of theory. In other words, only the positions of the H atom were optimized (in the X-ray crystallographic analysis, the positions of the H atoms were determined by calculations). On the basis of the optimized structure, TD-DFT calculations at the B3LYP/4333111/433111/4311[Sn],6-311G(2df,2p)[others] level of theory were performed. For comparison, TD-DFT calculations of $[K\cdot\mathbf{39}_3]^{2-}$ were also performed with the same method at the B3LYP/6-311G(2df,2p)//B3LYP/6-31G(d,p) level of theory.

As shown in the top of Fig. 27, the simulated spectra of $[K(thf)\cdot\mathbf{49}_3]^{2-}$ showed much more red-shifted absorption **c** with large oscillator strength at 565 nm as compared with that of **49**$^-$ (λ_{max} = 376 nm). In addition, absorptions **a** and **b** with small oscillator strength were found at 674 and 606 nm, respectively. The absorption at approximately 565 nm was reasonable one for a purple color of $K^+(thf)\cdot\mathbf{49}^-$ in the solid state. Although the red-shifted absorption was calculated for the germanium case $\mathbf{39}^-/[K\cdot\mathbf{39}_3]^{2-}$, the shift and the oscillator strengths of the corresponding absorptions were smaller than those in the tin case.

Electronic transitions corresponding to the absorptions **a**–**c** (Sn) and **a**–**d** (Ge) are shown at the bottom of Fig. 27. The HOMOs of $[K(thf)\cdot\mathbf{49}_3]^{2-}$ and $[K\cdot\mathbf{39}_3]^{2-}$ expanded to rings A(A) and B(B). Dominant absorptions **c** (Sn) and **d** (Ge) corresponded to the transitions from the HOMOs to the π-type orbitals, which also expanded to rings A(A) and B(B), LUMO+2 (Sn)/LUMO+3 (Ge). In the LUMO+2 (Sn)/LUMO+3 (Ge), the lobes on the Sn···Sn or Ge···Ge moieties were found, and this type of through-space interactions are considered important for the color in the solid state. The absorptions **a**,**b** (Sn)/**a**–**c** (Ge) with a longer wavelength and smaller oscillator strength than those of **c** (Sn) and **d** (Ge) corresponded mainly to the charge-transfer transitions from the HOMOs to the π-type orbitals, which expanded to rings C(C).

Although at this stage we cannot conclude the reasons for the color difference of $K^+(thf)\cdot\mathbf{49}^-$ between the solid and solution states, the through-space interaction between two SnC_5 rings *via* the Sn···Sn moiety in the solid state might be one of them.

5. Studies on the reactivity of germabenzenyl anions

As described in the previous sections, metallabenzenyl anions **39**$^-$ and **49**$^-$ were successfully synthesized and isolated. The spectroscopic and X-ray crystallographic analyses, in combination with theoretical calculations, indicated an ambident character of these metallabenzenyl anions, with contributions reflecting metallaaromatic and metallylene resonance structures.

To reveal unique reactivity and investigate the chemical properties of germabenzenyl anions **37**$^-$ and **39**$^-$, several reactions were performed. Here, we describe the results of the reaction study on $K^+\cdot\mathbf{39}^-$ due to its higher thermal stability as compared with that of $K^+\cdot\mathbf{37}^-$.

5.1. Reactions with electrophilic reagents. The reactions of $K^+\cdot\mathbf{39}^-$ with several electrophilic agents were performed. Although phenyllithium is known to undergo a nucleophilic substitution reaction with electrophilic agents, it is known that some

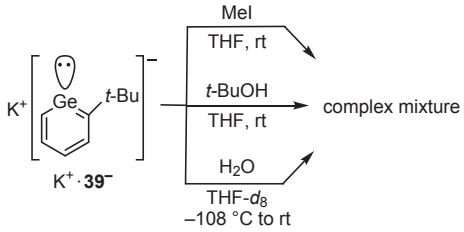

Scheme 17. Reactions of $K^+ \cdot \mathbf{39}^-$ with iodomethane and several proton sources.

germylenes insert into active σ-bonds such as carbon–halogen bonds.

The reaction of $K^+ \cdot \mathbf{39}^-$ with an excess amount of iodomethane in THF was found to afford a complicated mixture that is insoluble in organic solvents such as hexane, benzene, THF, and ethyl acetate (Scheme 17). It could be considered that the neutral products bearing small methyl groups are thermally unstable and undergo self-oligomerization.

Although the protonation of $K^+ \cdot \mathbf{39}^-$ was also performed, treatment of $K^+ \cdot \mathbf{39}^-$ with H_2O and *tert*-butyl alcohol as a proton source in THF-d_8 gave an intractable mixture without any evidence for the generation of the expected hydrogen-substituted germabenzene (Scheme 17).

Next, the reaction with chlorotrimethylsilane, which has a bulkier trimethylsilyl group than the methyl group, was examined in expectation of suppressing the oligomerization of the products. Treatment of $K^+ \cdot \mathbf{39}^-$ with an excess amount of chlorotrimethylsilane in THF gave a mixture of **52** and **53** (2:1 ratio), the [4 + 2] dimers of trimethylsilyl-substituted germabenzene **55** (Scheme 18).[81]

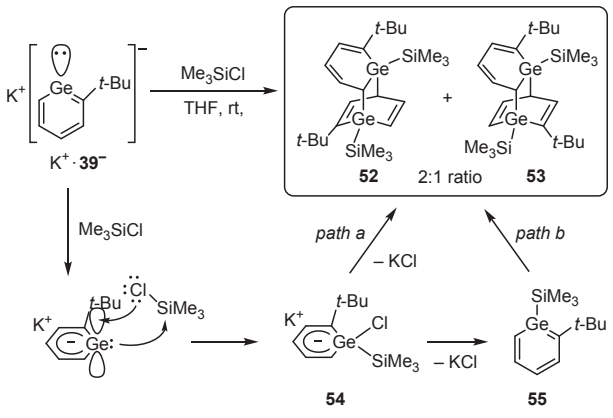

Scheme 18. Reaction of $K^+ \cdot \mathbf{39}^-$ with chlorotrimethylsilane, together with a plausible mechanism.

Although it is difficult to separate and isolate these isomers because of their very similar physical properties and low crystallinity, their structures were determined based on the measurements of correlation spectroscopy (COSY) and nuclear Overhauser effect spectroscopy (NOESY), together with high-resolution mass spectroscopy.

On the basis of the frontier orbital theory, as a plausible mechanism, this reaction is considered to proceed *via* the interaction between the vacant p-orbital of the germanium atom that appeared on the LUMO and lone pair on the chlorine atom, giving the insertion product **54**. There are two possibilities for the final step, namely, the double nucleophilic substitution of anions **54** (*path a*) and the dimerization of germabenzene **55** formed by the KCl elimination from **54** (*path b*). However, *path a* would be unfavorable because of the steric hindrance in the formation of the penta-coordinated intermediate and the electronic repulsion between anions, and the transformation from **54** to **55** would be advantageous because of the high aromatization energy. At this stage, therefore, trimethylsilyl-substituted germabenzene **55** might be the possible intermediate to give the dimers in this reaction.

Next, the protonation of $\mathbf{39}^-$ in a nonpolar solvent was investigated from the viewpoint of the effect of solvent polarity, and K^+(crypt-222)$\cdot \mathbf{39}^-$ was selected as the substrate for this reaction because of the insolubility of $K^+ \cdot \mathbf{39}^-$ in hydrocarbon solvents. The reaction of K^+(crypt-222)$\cdot \mathbf{39}^-$ with an excess amount of H_2O in C_6D_6 afforded a mixture of **56** and **57**. ^{1}H NMR spectroscopy indicated that the initial products ratio should be 7:3 (**56**:**57**), and compound **56** gradually changed into thermally stable isomer **57** after standing of the crude products in C_6D_6 for several days (Scheme 19).

As in the case of the reaction with chlorotrimethylsilane, the initial step in this reaction is considered to be the interaction between the vacant p-orbital of the germanium atom and the lone pair on the oxygen atom, followed by the insertion reaction into the O–H bond. In this reaction, anion **58** was treated with a large amount of H_2O, which resulted in the cleavage of the Ge–C bond and the formation of a mixture of **56** and **57** (Scheme 20).

5.2. Investigation of reactivity as a germylene. Triethylsilane is known as an effective trapping reagent for germylenes.[82] However, the reaction of $K^+ \cdot \mathbf{39}^-$ with triethylsilane in THF-d_8 resulted in no reaction even under a heated condition (Scheme 21). Because the Si–H insertion reaction of

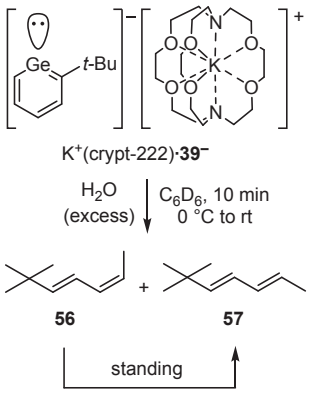

Scheme 19. Reaction of K^+(crypt-222)·**39**$^-$ with H_2O in C_6D_6.

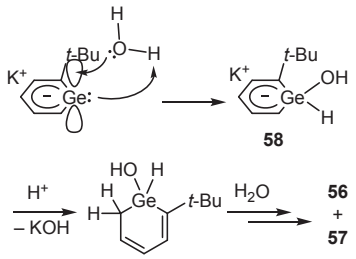

Scheme 20. Plausible mechanism for the reaction of K^+(crypt-222)·**39**$^-$ with H_2O in C_6D_6.

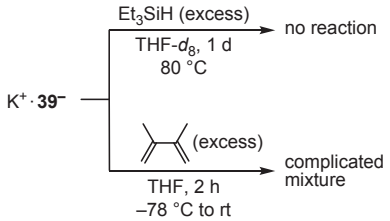

Scheme 21. Reactions of K^+·**39**$^-$ with triethylsilane and 2,3-dimethyl-1,3-butadiene.

a germylene is proposed to occur in a concerted manner *via* a three-membered-ring transition state, the LUMO in **39**$^-$ might be more stabilized than the typical germylenes.

Conversely, treatment of K^+·**39**$^-$ with 2,3-dimethyl-1,3-butadiene, which is also commonly used as an effective trapping reagent for germylenes, proceeded but gave a complicated mixture (Scheme 21).

5.3. Reactions with transition metals. Heavy aromatics are expected to serve as a new class of ligands for transition metal complexes due to their extended π-orbitals on the ring skeleton at higher energy levels than the corresponding parent hydrocarbons. For example, considerable interest has been focused on transition metal complexes incorporating heavy cyclopentadienides[83] such as $[SiC_4R_5]^-$,[84] $[GeC_4R_5]^-$,[84a),85] $[Si_3C_2R_5]^-$,[86] and $[Si_2GeC_2R_5]^-$,[87] coordinated with an η^5-fashion-like cyclopentadienide ion (Cp^-). More recently, dianions of stannole ($[SnC_4R_4]^{2-}$)[88] and plumbole ($[PbC_4R_4]^{2-}$)[89] were also reported to coordinate with transition metals in various fashions. Heavy cyclobutadienes with SiC_3,[90] Si_3Ge,[91] Si_4,[91),92] and Ge_4[93] cores are also known to coordinate with transition metals as a 6π-aromatic ligand by two-electron donation from the metal. In this context, we have also demonstrated that sila- and germabenzenes 1-Tbt-EC_5H_5 (E = Si, Ge) act as an η^6-arene ligand toward Group 6 metals despite the presence of an extremely bulky substituent.[94] Conversely, arenyl anions, *i.e.*, anionic arenyl units such as phenyllithium, are widely used organometallic reagents mostly as building blocks for the synthesis of metallated arenyl complexes *via* addition or substitution reactions. As described previously, in most cases, the phenyl anion can coordinate with transition metals in an η^1 fashion due to its σ-type HOMO at the anionic carbon atom. π-Coordination from the anionic arenyl unit would be unfavorable because of its low-energy p-orbitals and the resulting loss of aromaticity upon coordination.

Because it was revealed that germabenzenyl anion **39**$^-$ exhibited significant contributions of both a germylene-type structure supported by an anionic C_5 backbone and a character of heavy aromatics (as well as phenyl anion), we became interested in the complexation behavior of **39**$^-$ toward transition metals and performed the reaction of K^+·**39**$^-$ with $[Cp^*RuCl]_4$, leading to the corresponding ruthenium complexes **59** and **60** having unique coordination modes of GeC_5 rings.[95] Treatment of K^+·**39**$^-$ with 0.25 equivalents of $[Cp^*RuCl]_4$ at ambient temperature in THF afforded ruthenium complexes **59** and **60** in 13% and 23% yields, respectively, as stable orange crystals (Scheme 22). Complexes **59** and **60** exhibited both σ- and π-type coordination, and it is noteworthy that they can be regarded as the first examples of a transition-metal-substituted benzenoid of heavier Group 14 elements.

Although **59** and **60** were highly sensitive to air and moisture, they both exhibited high thermal stability in the solid state under an inert atmosphere. X-Ray crystallographic analysis unambiguously determined the molecular structures of **59** and **60** as the dimer and trimer of a $[Cp^*Ru(GeC_5(t\text{-}Bu)H_4)]$ unit, respectively (Fig. 28).

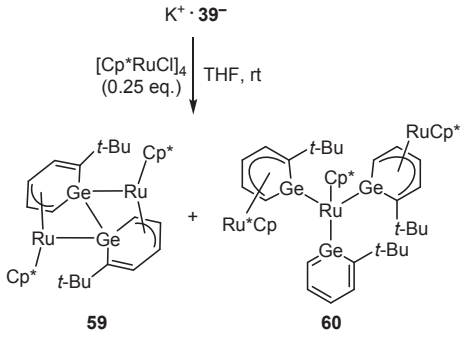

Scheme 22. Reaction of $K^+ \cdot \mathbf{39}^-$ with $[Cp^*RuCl]_4$.

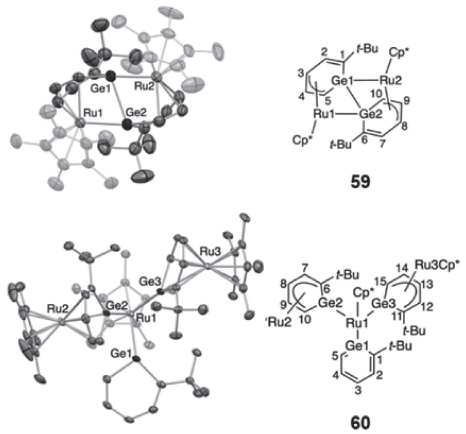

Fig. 28. Thermal ellipsoid plots (50% probability) for **59** and [**60**·0.5benzene]. The hydrogen atoms and benzene molecules were omitted for clarity. (*Chem. Commun.* **2018**, 8044–8047)

Complex **59** had an almost C_2 symmetrical Ge_2Ru_2 core, the GeC_5 rings of which were significantly distorted and coordinated with the ruthenium atoms in η^1 and η^3 fashions. On the basis of the comparison of the Ge–Ru distances of **59** with those of the related compounds,[85a),94d),96),97)] it was assumed that the Ru1 and Ru2 atoms, at least from the structural aspect, were coordinated by the C3–C5 and C8–C10 moieties, respectively, similarly to common η^3-π-allyl ligands. In addition, the Ge1–Ge2 bond distance [2.5053(7) Å] of **59** was close to the distances of Ge–Ge single bonds in other known compounds containing Group 8 transition metals (2.45–2.55 Å),[98)] suggesting that complex **59** had a Ge–Ge single-bond character.

Complex **59** was characterized also using ^{1}H and ^{13}C NMR, and UV–vis spectroscopy. The ^{1}H and ^{13}C NMR chemical shifts for H3, H4, H5, C3, C4, and C5 of the GeC_5 ring moiety of **59** were clearly upfield-shifted relative to those of 2-*t*-butyl-1-Tbt-germabenzene **38** and $K^+ \cdot \mathbf{39}^-$. These high-field shifts in **59** were most likely caused by π back-donation from the ruthenium atoms to the GeC_5 ring moiety, suggesting that the Ru1 and Ru2 atoms interacted with C3, C4, and C5 and C8, C9, and C10, respectively, in an η^3 fashion. These results are in good agreement with the partial coordination of the GeC_5 ring shown by the X-ray crystallographic analysis and indicate the retention of the solid-state coordination mode even in solution.

Owing to the poor solubility and instability of complex **60**, we could not determine the nature of **60** in solution even using an 800 MHz NMR spectrometer with CryoProbe. However, the molecular structure of **60** in the solid state was established by the crystallographic analysis of a single crystal of [**60**·0.5benzene] (Fig. 28). In complex **60**, although two of the GeC_5 rings ($Ge2C_5$ and $Ge3C_5$) interacted with two ruthenium atoms *via* σ- and π-type coordination, the $Ge1C_5$ ring was free from the π-type coordination and coordinated with Ru1 only in the η^1 fashion.

In addition, theoretical calculations for geometry optimization and frequency calculations were conducted for the corresponding monomeric structures **61** (η^6), **61** (η^1), [**62**·thf] (η^1), and [**62**·2thf] (η^1) (Fig. 29). Although the calculated chemical shifts using the optimized structure of **59** showed a similar trend to that of the observed ones, the calculated chemical shifts for the corresponding monomeric structures for **61** and **62** were quite different from

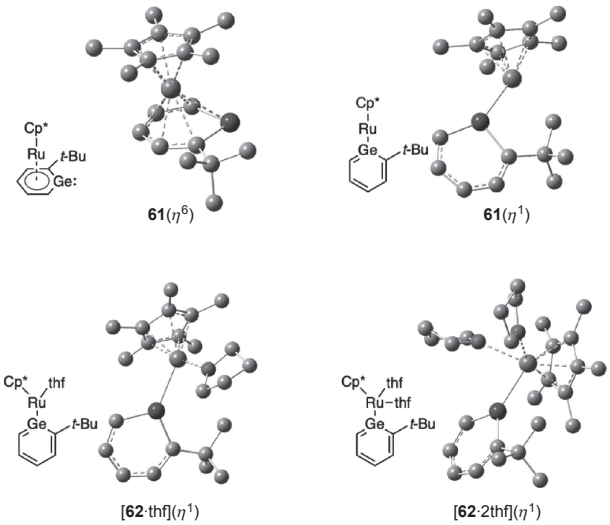

Fig. 29. Optimized structures for **61** (η^6), **61** (η^1), [**62**·thf] (η^1), and [**62**·2thf] (η^1). Hydrogen atoms were omitted for clarity. (*Chem. Commun.* **2018**, 8044–8047)

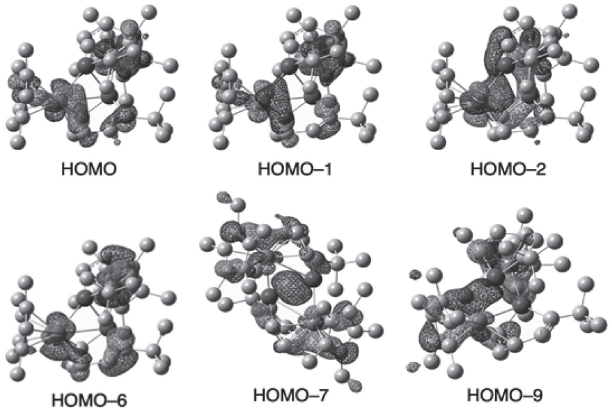

Fig. 30. Molecular orbitals of **59** (isovalue = 0.04). HOMO [p(C3,C8)–d(Ru)], HOMO–1 [p(C3,C8)–d(Ru)], HOMO–2 [p(C5,C10)–d(Ru)], HOMO–6 [p(C3–C4, C8–C9)–d(Ru)], HOMO–7 [σ(Ge1–Ge2)], and HOMO–9 [p(Ge1,Ge2)–d(Ru)]. (*Chem. Commun.* **2018**, 8044–8047)

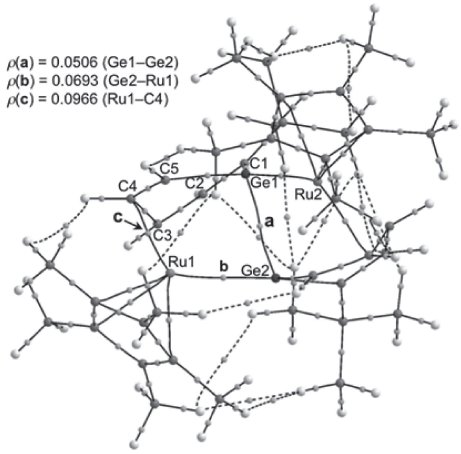

Fig. 31. BCPs and BPs in complex **59**. (*Chem. Commun.* **2018**, 8044–8047)

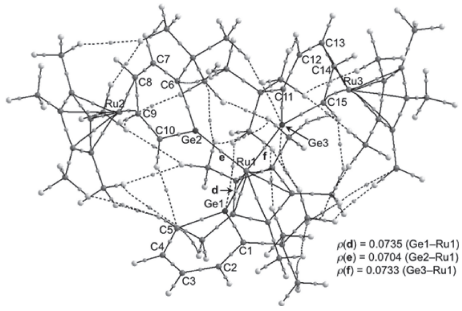

Fig. 32. BCPs and BPs in complex **60**. (*Chem. Commun.* **2018**, 8044–8047)

those observed. Moreover, upon the addition of triphenylphosphine or THF to a C_6D_6 solution of **59**, no change and no coordination were observed in the ^{1}H NMR spectra. Furthermore, **59** showed no change for the ^{1}H NMR spectra in the ranges of 20 °C to 60 °C (in benzene-d_6) and −70 °C to 60 °C (in THF-d_8) and for the UV−vis spectra in the range of 20 °C to 50 °C (in hexane or THF). These results suggest that complex **59** remained a dimeric structure even in solution.

To understand the electronic structure of complex **59**, theoretical calculations for **59** were performed using the Gaussian 09 program. Selected MOs of importance are shown in Fig. 30.

The HOMO, HOMO–1, HOMO–2, and HOMO–6 mainly consisted of ruthenium-based d-orbitals and p-orbitals of C3–C5 and C8–C10, respectively, in the GeC_5 ring. The HOMO–7 contained the Ge1–Ge2 σ-bonding interaction, in agreement with the short interatomic distance found in **59**. Moreover, the Ge atom had an η^1 interaction with the Ru atom, which was found in the HOMO–9, but significant π-type interactions between the Ge and Ru atoms were not observed. It is concluded that the GeC_5 moiety coordinates to the ruthenium atoms in both η^1 and η^3 fashions.

These results are clearly supported by the atoms in molecules (AIM) calculations, and the bond critical points (BCPs) and bond paths (BPs) found for complexes **59** and **60** are shown in Figs. 31 and 32. Bond critical points (BCPs) and bond paths (BPs) were found between the two Ge atoms. In complex **59**, the BCPs and BPs were found between Ge1–Ru2 and Ge2–Ru1 and no BCP and BP were found between Ge1–Ru1 and Ge2–Ru2.

As for the $Ge1C_5$ ring of complex **60**, the sum of the interior bond angles was 720.0°, indicating the high planarity of the ring. Although the lengths of the Ge–C bonds in $Ge1C_5$, Ge1–C1 [1.918(3) Å] and Ge1–C5 [1.900(3) Å], were longer than the corresponding bonds in 2-*t*-butyl-1-Tbt-germabenzene **38** [Ge–C = 1.851(3), 1.847(4) Å], they were similar to or shorter than those in aromatic germabenzenyl anion **39**$^-$. In addition, the difference in the two Ge–C bond lengths in the $Ge1C_5$ ring became smaller than the differences in the other GeC_5 rings of **60** and the GeC_5 rings of **59** and **39**$^-$. The lengths of the four C–C bonds [1.386(5)–1.398(5) Å] were almost the same as those in **38** [C–C = 1.368(6)–1.396(5) Å]. The observed planar structure of $Ge1C_5$, which exhibited unsaturated bonds with virtually no bond alternation, was thus in agreement with the structural criteria for aromaticity. That is to say, complex **60** can be ascribed as a ruthenium-substituted

germabenzene, the first example of thermally stable heavy benzene having a transition metal substituent on the heavy element.

On the contrary, the sums of the interior bond angles of the $Ge2C_5$ and $Ge3C_5$ rings of **60** were 718.8° and 716.5°, respectively, and the deviations of the Ge atom from the C_5 plane were 0.214 Å (Ge2) and 0.383 Å (Ge3), showing the nonplanarity of the rings and the small flipping of the Ge atoms from the C_5 planes. Although the lengths of Ru1–Ge1, Ru1–Ge2, and Ru1–Ge3 [2.4167(4)–2.4482(4) Å] in η^1-coordination modes were in the range of previously reported Ge–Ru bond lengths (2.442–2.549 Å), those of Ru2–Ge2 [2.7800(4) Å] and Ru3–Ge3 [2.8682(4) Å] were longer than those mentioned above and close to those in **59** (Ge1–Ru1/Ge2–Ru2). The Ge–C bond lengths in $Ge2C_5$ and $Ge3C_5$ (Ge2–C6 [1.968(3) Å], Ge2–C10 [1.925(3) Å], Ge3–C11 [1.957(3) Å], and Ge3–C15 [1.929(3) Å]) were close to those in **59** and longer than those in $Ge1C_5$ of **60**. The four C–C bonds in their rings [1.402(5)–1.423(5) Å ($Ge2C_5$) and 1.405(5)–1.423(5) Å ($Ge3C_5$)] were much longer than those in **38** and similar to those in ruthenium complexes containing cyclohexadienyl and pentadienyl ligands (1.39–1.44 Å). The elongation seemed to be due to the back-donation from ruthenium atoms to the GeC_5 ring moieties. From these structural aspects, it can be concluded that the $Ge2C_5$ and $Ge3C_5$ rings of complex **60** coordinated with the Ru atoms as η^5-germacyclohexadienyl and η^1-germylene ligands and there was no significant π-bond between the Ge and C atoms.

The molecular orbitals (MOs) of **60** and the parent germabenzene ($HGeC_5H_5$) are summarized in Fig. 33. Three π-type MOs analogous to those of $HGeC_5H_5$ on the $Ge1C_5$ moiety were found and filled with six π-electrons. In addition, NBO calculations for **60** using NBO 6.0 showed the π-bond between the Ge1 and C5 atoms.[95] These results clearly showed that the orbital situation on the $Ge1C_5$ moiety could be described as germabenzene. However, no π-bonds between the Ge2/Ge3 and C atoms and no BCPs on Ge2–Ru2 and Ge3–Ru3 were found in the results of the NBO and AIM (Fig. 32) calculations, respectively, supporting their η^1,η^5-coordination mode as described above. The hybridizations of the Ge atom on the Ge–Ru1 bonds were calculated as $sp^{1.24}$ (Ge1), $sp^{0.56}$ (Ge2), and $sp^{0.30}$ (Ge3). The high s-characters of Ge2 and Ge3 indicated their germylene-type coordination in complex **60**.

5.4. Reactions with chalcogen donors. To obtain the germanium congeners of potassium phenoxide bearing GeX^- (X = chalcogen), we examined the reaction of germabenzenylpotassium $K^+\cdot$**39**$^-$ with chalcogen donors.

When $K^+\cdot$**39**$^-$ was treated with an excess amount of N_2O, an extensively used oxygen donor, in THF-d_8, purple precipitates were obtained but the products were insoluble in common organic solvents and very complicated to be identified (Scheme 23).

Conversely, the reaction of K^+(18-c-6)·**39**$^-$ with a stoichiometric amount of N_2O in benzene resulted in the formation of product **63**, which is a dimer of the germanium analog of potassium phenoxide, in 67% yield (Scheme 23). Compound **63** was isolated as highly moisture-sensitive colorless crystals and characterized using NMR spectroscopy and X-ray crystallographic analysis (Fig. 34).

The formation of the dimer of heavy phenoxide **63** is worthy of mention as a unique example of the application of metallabenzenyl anions to the development of a new building block based on heavy aromatic skeletons.

5.5. Summary of the reactivity of metallabenzenyl anions. In this section, we examined the reactivity of germabenzenyl anion **39**$^-$ as a model of heavy metallabenzenyl anions. The reaction of

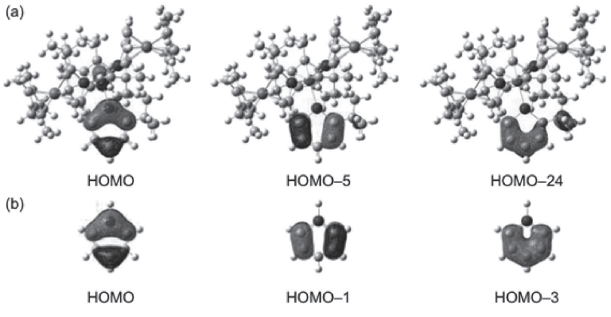

Fig. 33. Molecular orbitals (isovalue = 0.04) of complex **60** (a) and the parent germabenzene, $HGeC_5H_5$ (b). (*Chem. Commun.* **2018**, 8044–8047)

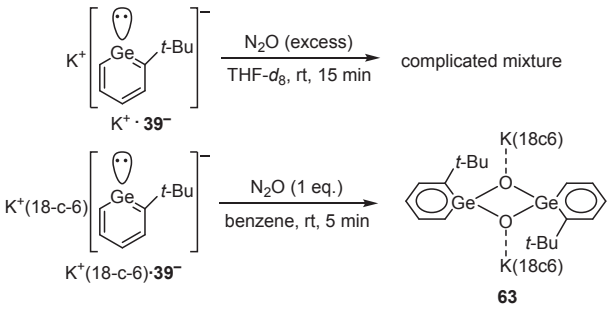

Scheme 23. Reactions of $K^+\cdot$**39**$^-$ and K^+(18-c-6)·**39**$^-$ with N_2O.

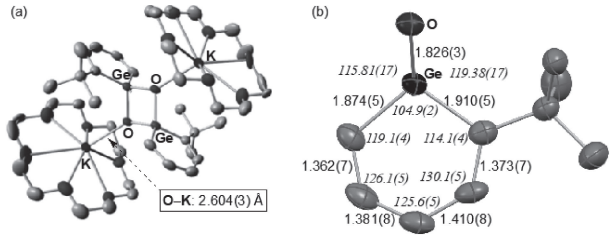

Fig. 34. (a) Atomic displacement parameter plots for **63** with thermal ellipsoids set at 50% probability. (b) Selected bond lengths [Å] and angles [°] (in italics) in **63**.

K^+·**43**$^-$ with chlorotrimethylsilane afforded the mixture of **52** and **53**, the [4 + 2]-dimers of trimethylsilyl-substituted germabenzene **55**. On the basis of the frontier orbital theory, the initial step of this reaction is considered to proceed *via* the interaction between the vacant p-orbital of the germanium atom that appeared on the LUMO and the lone pair on the chlorine atom, giving insertion product **54**. As in the case of chlorotrimethylsilane, the initial step of the reaction with H_2O is considered to proceed *via* the interaction between the vacant p-orbital of the germanium atom and the lone pair on the oxygen atom. Conversely, the reaction of K^+·**39**$^-$ with triethylsilane, which is known as a trapping reagent for germylenes, resulted in no reaction even under heated conditions. This result suggested that the LUMO in germabenzenyl anion **39**$^-$ is considered more stabilized than the typical germylenes. Furthermore, complexation of K^+·**39**$^-$ with $[Cp^*RuCl]_4$ resulted in the formation of two types of ruthenium complexes **59** and **60** having unique coordination modes. Complexes **59** and **60** exhibited both σ- and π-type coordination, and they can be regarded as the first examples of transition-metal-substituted benzenoid of heavier Group 14 elements. In the case of oxygenation using N_2O, K^+(18-c-6)·**39**$^-$ was found to give the dimer of the corresponding heavy phenoxide **63**. Thus, it was demonstrated that K^+·**39**$^-$ showed several unique reactivities beneficial for application in the development of new organogermanium species.

6. Conclusion and outlook

In this work, we synthesized and isolated the first "heavy phenyl anions", which are the heavier Group 14 element analogs of phenyl anions, by taking advantage of the stabilization afforded by charge repulsion instead of steric protection.

In the case of germanium, that is, the germanium analogs of phenyl anions, the reactions of the corresponding stable germabenzene with reducing agents resulted in the formation of the target germabenzenyl anions under the concomitant elimination of the aryl group from the Ge atom. In the crystalline state, as well as in solution, the germabenzenyl moiety adopted a monomeric form, even though the X-ray diffraction analysis suggested the presence of highly reactive Ge=C double bonds. The spectroscopic and X-ray crystallographic analyses, in combination with theoretical calculations, indicated an ambident character of this germabenzenyl anion, with contributions from aromatic and germylene resonance structures.

Next, we extended this chemistry to the synthesis and isolation of the stannabenzenyl anion, the first stable tin-containing benzene derivative, by utilizing the same strategy employed for the germanium system. The properties were revealed by X-ray crystallographic analysis, NMR and UV–vis spectroscopy, and theoretical calculations, indicating that the stannabenzenyl anion also showed both a stannylene character and an aromatic character. It should also be noted that by this extension, this new stabilization strategy utilizing electronic repulsion was found to be a promising method for isolating highly reactive species.

In addition, we conducted research on the reactivity of the metallabenzenyl anions using a germabenzenyl anion as a substrate. The reaction of a germabenzenylpotassium with chlorotrimethylsilane as an electrophilic agent afforded the [4 + 2] dimers of the intermediary trimethylsilyl-substituted germabenzene. In the complexation with $[Cp^*RuCl]_4$, two types of ruthenium complexes having unique coordination modes were obtained. On the basis of the frontier orbital theory, the initial step of these reactions is considered to proceed *via* the interaction between the vacant p-orbital of the germanium atom and the lone pair on the chlorine atom. It should be noted that the germabenzenyl anion was found to be available as a building block for the introduction of a germabenzene moiety.

Further studies are currently in progress to extend this novel concept of stabilization for highly reactive species based on "electronic repulsion" toward a silabenzenyl anion and polycyclic aromatic hydrocarbon anionic systems of heavier Group 14 elements such as 2-metallanaphthalenyl and 9-metallaanthracenyl skeletons. We believe that the knowledge obtained in this research should make a great contribution to the progress of organoelement chemistry and should lead to a novel design of functional

π-conjugated systems combined with heavier main group elements.

Acknowledgements

This work was supported by JSPS KAKENHI Grant Numbers JP19H05635, JP19H05528, JP18H01963, and JP16H4110 and Integrated Research Consortium on Chemical Science. Y.M. gratefully acknowledges ISHIZUE 2022 of Kyoto University. This study was supported by the Joint Usage/ Research Center [Institute for Chemical Research (ICR), Kyoto University] by providing access to a Bruker Avance III 600 NMR spectrometer. We are furthermore grateful for computation time, which was provided by the Super Computer Laboratory (ICR, Kyoto University). Elemental analyses were conducted at the Microanalytical Laboratory of the ICR (Kyoto University).

References

1) Minkin, V.J., Glukhovtsev, M.N. and Simkin, Y.B. (1994) Aromaticity and Antiaromaticity; Electronic and Structure Aspects. Wiley, New York.
2) Faraday, M. (1825) XX. On new compounds of carbon and hydrogen, and on certain other products obtained during the decomposition of oil by heat. Phil. Trans. Roy. London **115**, 440–466.
3) Mitscherlich, E. (1834) Über das Benzol und die Säuren der Oel- und Talgarten. Ann. Pharm. **9**, 39–48.
4) (a) Kekulé, F.A. (1865) Sur la constitution des substances aromatiques. Bull. Soc. Chim. Paris **3**, 98–110. (b) Kekulé, F.A. (1866) Untersuchungen uber aromatische Verbindungen. Liebigs Ann. Chem. **137**, 129–196.
5) (a) Pauling, L. (1931) The nature of the chemical bond. Application of results obtained from the quantum mechanics and from a theory of paramagnetic susceptibility to the structure of molecules. J. Am. Chem. Soc. **53**, 1367–1400. (b) Pauling, L. (1932) Interatomic distances in covalent molecules and resonance between two or more Lewis electronic structures. Proc. Natl. Acad. Sci. U.S.A. **18**, 293–297. (c) Pauling, L., Brockway, L.O. and Beach, J.Y. (1935) The dependence of interatomic distance on single bond-double bond resonance. J. Am. Chem. Soc. **57**, 2705–2709.
6) (a) Jeffrey, G.A., Ruble, J.R., McMullan, R.K. and Pople, J.A. (1987) The crystal structure of deuterated benzene. Proc. R. Soc. Lond. A **414**, 47–57. (b) Ermer, O. (1987) Concerning the structure of benzene. Angew. Chem. Int. Ed. Engl. **26**, 782–784. (c) Cox, K.E.G., Cruickshank, D.W. and Smith, J.A.S. (1958) The crystal structure of benzene at −3 °C. Proc. R. Soc. Lond. A **247**, 1–21. (d) Bacon, G.E., Curry, N.A. and Wilson, S.A. (1964) A crystallographic study of solid benzene by neutron diffraction. Proc. R. Soc. Lond. A **279**, 98–110.
7) (a) Kruszewski, J. and Krygowski, T.M. (1972) Definition of aromaticity basing on the harmonic oscillator model. Tetrahedron Lett. **13**, 3839–3842. (b) Krygowski, T.M. and Cyrañski, M.K. (1996) Separation of the energetic and geometric contributions to the aromaticity. Part IV. A general model for the π-electron systems. Tetrahedron **52**, 10255–10264. (c) Krygowski, T.M. and Cyrañski, M.K. (2001) Structural aspects of aromaticity. Chem. Rev. **101**, 1385–1419.
8) Schleyer, P.v.R., Maerker, C., Dransfeld, A., Jiao, H. and van Eikema Hommes, N.J.R. (1996) Nucleus-independent chemical shifts: A simple and efficient aromaticity probe. J. Am. Chem. Soc. **118**, 6317–6318.
9) Chen, Z., Wannere, C.S., Corminboeuf, C., Puchta, R. and Schleyer, P.v.R. (2005) Nucleus-independent chemical shifts (NICS) as an aromaticity criterion. Chem. Rev. **105**, 3842–3888.
10) (a) Hehre, W.J., Ditchfield, R., Radom, L. and Pople, J.A. (1970) Molecular orbital theory of the electronic structure of organic compounds. V. Molecular theory of bond separation. J. Am. Chem. Soc. **92**, 4796–4801. (b) George, P., Trachtman, M., Bock, C.W. and Brett, A.M. (1976) Homodesmotic reactions for the assessment of stabilization energies in benzenoid and other conjugated cyclic hydrocarbons. J. Chem. Soc., Perkin Trans. **2**, 1222–1227.
11) (a) Hehre, W.J., McIver, R.T., Pople, J.A. and Schleyer, P.v.R. (1974) Alkyl Substituent effects on the stability of protonated benzene. J. Am. Chem. Soc. **96**, 7162–7163. (b) Radom, L. (1974) Ab initio molecular orbital calculations on anions. Determination of gas phase acidities. J. Chem. Soc. Chem. Commun. **10**, 403–404. (c) George, P., Trachtman, M., Brett, A.M. and Bock, C.W. (1977) Comparison of various isodesmic and homodesmotic reaction heats with values derived from published *ab initio* molecular orbital calculations. J. Chem. Soc., Perkin Trans. **2**, 1036–1047.
12) Schleyer, P.v.R. and Jiao, H. (1996) What is aromaticity? Pure Appl. Chem. **68**, 209–218.
13) (a) Solouki, B., Rosmus, P., Bock, H. and Maier, G. (1980) Short-path pyrolysis: Silabenzene. Angew. Chem. Int. Ed. Engl. **19**, 51–52. (b) Maier, G., Mihm, G. and Reisenauer, H.P. (1980) Silabenzene. Angew. Chem. Int. Ed. Engl. **19**, 52–53.
14) (a) Maier, G., Mihm, G. and Reisenauer, H.P. (1982) Thermische Dehydrierung von 1-Sila-2,5-cyclohexadien zu Silabenzol. Chem. Ber. **115**, 801–803. (b) Maier, G., Mihm, G., Baumgärtner, R.O.W. and Reisenauer, H.P. (1984) Hetero-p-Systeme, 7. Silabenzol. Chem. Ber. **117**, 2337–2350.
15) (a) Märkl, G. and Hofmeister, P. (1979) 1,4-Di-*tert*-butylsilabenzene: Generation and trapping reactions. Angew. Chem. Int. Ed. Engl. **18**, 789–790. (b) Märkl, G. and Rudnick, D. (1980) 1.4-di-*tert*-butyl-germabenzol-erzeugung und abfangreaktionen germabenzol- und 1.2-dihydrogermabenzol-

dimere. Tetrahedron Lett. **21**, 1405–1408.
16) Märkl, G. and Schlosser, W. (1988) 1,4-Di-*tert*-butyl-2,6-bis(trimethylsilyl)silabenzene, the first silabenzene stable in solution at −100 °C. Angew. Chem. Int. Ed. Engl. **27**, 963–965.
17) Jutzi, P., Meyer, M., Reisenauer, H.P. and Maier, G. (1989) Zur kinetischen Stabilisierung von Silabenzol: Matrix-Isolierung und Charakterisierung von 2,4,6-Tris(trialkylsilyl)-substituiertem 1-*tert*-Butyl-1-silabenzol. Chem. Ber. **122**, 1227–1230.
18) Windus, T.L. and Gordon, M.S. (1992) π-Bond strengths of $H_2X = YH_2$: X = Ge, Sn; Y = C, Si, Ge, Sn. J. Am. Chem. Soc. **114**, 9559–9568.
19) (a) Okazaki, R., Unno, M. and Inamoto, N. (1987) 2,4,6-Tris(bis(trimethylsilyl)methyl)phenyl, a new sterically demanding group for kinetic stabilization of unstable compounds. Chem. Lett. **16**, 2293–2294. (b) Okazaki, R., Unno, M. and Inamoto, N. (1989) Estimation of bulkiness of a highly sterically demanding 2,4,6-Tris[bis(trimethylsilyl)-methyl]phenyl Group. Chem. Lett. **18**, 791–792. (c) Okazaki, R., Tokitoh, N. and Matsumoto, T. (1996) 5,5-Diaryl-1,2,3,4,5-tetrathiagermolanes, diarylgermanethiones; Ar, (Ar.′)GeS_4, Ar(Ar′)Ge = S. *In* Synthetic Methods of Organometallic and Inorganic Chemistry (Herman, W.A., Auner, N. and Klingebiel, U. Eds.). Thieme, New York, Vol. 2, pp. 260–269.
20) (a) Tokitoh, N., Matsuhashi, Y., Shibata, K., Matsumoto, T., Suzuki, H., Saito, M. *et al.* (1994) New aspects in the chemistry of low-coordinate compounds of group 14 elements. Main Group Met. Chem. **17**, 55–65. (b) Tokitoh, N., Matsumoto, T. and Okazaki, R. (1999) The chemistry of germanium-containing heavy ketones. Bull. Chem. Soc. Jpn. **72**, 1665–1684. (c) Okazaki, R. and Tokitoh, N. (2000) Heavy ketones, the heavier element congeners of a ketone. Acc. Chem. Res. **33**, 625–630.
21) (a) Sugiyama, Y., Sasamori, T., Hosoi, Y., Furukawa, Y., Takagi, N., Nagase, S. *et al.* (2006) Synthesis and properties of a new kinetically stabilized digermyne: New insights for a germanium analogue of an alkyne. J. Am. Chem. Soc. **128**, 1023–1031. (b) Sasamori, T., Hironaka, K., Sugiyama, Y., Takagi, N., Nagase, S., Hosoi, Y. *et al.* (2008) Synthesis and reactions of a stable 1,2-diaryl-1,2-dibromodisilene: A precursor for substituted disilenes and a 1,2-diaryldisilyne. J. Am. Chem. Soc. **130**, 13856–13857.
22) (a) Tokitoh, N., Arai, Y., Sasamori, T., Okazaki, R., Nagase, S., Uekusa, H. *et al.* (1998) A unique crystalline-state reaction of an overcrowded distibene with molecular oxygen: The first example of a single crystal to a single crystal reaction with an external reagent. J. Am. Chem. Soc. **120**, 433–434. (b) Tokitoh, N., Arai, Y., Okazaki, R. and Nagase, S. (1997) Synthesis and characterization of a stable dibismuthene: Evidence for a Bi-Bi double bond. Science **277**, 78–80. (c) Sasamori, T., Arai, Y., Takeda, N., Okazaki, R., Furukawa, Y., Kimura, M. *et al.* (2002) Syntheses, structures and properties of kinetically stabilized distibenes and dibismuthenes, novel doubly bonded systems between heavier group 15 elements. Bull. Chem. Soc. Jpn. **75**, 661–675.
23) Sato, T., Mizuhata, Y. and Tokitoh, N. (2010) 1,2-Dialkynyldisilenes: silicon analogues of (E)-enediyne. Chem. Commun. (Camb.) **46**, 4402–4404.
24) (a) Okazaki, R. and Tokitoh, N. (2000) Heavy ketones, the heavier element congeners of a ketone. Acc. Chem. Res. **33**, 625–630. (b) Mizuhata, Y., Takeda, N., Sasamori, T. and Tokitoh, N. (2005) Synthesis and properties of a stable 6-stannapentafulvene. Chem. Commun. (Camb.) 5876–5878.
25) (a) Wakita, K., Tokitoh, N., Okazaki, R. and Nagase, S. (2000) Synthesis and properties of an overcrowded silabenzene stable at ambient temperature. Angew. Chem. Int. Ed. **39**, 634–636. (b) Wakita, K., Tokitoh, N., Okazaki, R., Takagi, N. and Nagase, S. (2000) Crystal structure of a stable silabenzene and its photochemical valence isomerization into the corresponding silabenzvalene. J. Am. Chem. Soc. **122**, 5648–5649.
26) Nakata, N., Takeda, N. and Tokitoh, N. (2002) Synthesis and properties of the first stable germabenzene. J. Am. Chem. Soc. **124**, 6914–6920.
27) (a) Kaiya, C., Suzuki, K. and Yamashita, M. (2019) Chlorine-substituted germabenzene: Generation and application as a precursor for aryl-substituted germabenzenes. Organometallics **38**, 610–613. (b) Kaiya, C., Suzuki, K. and Yamashita, M. (2019) A monomeric stannabenzene: Synthesis, structure, and electronic properties. Angew. Chem. Int. Ed. **58**, 7749–7752.
28) (a) Tokitoh, N. (2004) New progress in the chemistry of stable metallaaromatic compounds of heavier group 14 elements. Acc. Chem. Res. **37**, 86–94. (b) Takeda, N., Shinohara, A. and Tokitoh, N. (2002) Synthesis and properties of the first 1-silanaphthalene. Organometallics **21**, 4024–4026. (c) Tokitoh, N., Wakita, K., Okazaki, R., Nagase, S., Schleyer, P.v.R. and Jiao, H. (1997) A Stable Neutral Silaaromatic Compound, 2-{2,4,6-Tris[bis(trimethylsilyl)methyl]phenyl}-2-silanaphthalene. J. Am. Chem. Soc. **119**, 6951–6952. (d) Nakata, N., Takeda, N. and Tokitoh, N. (2003) Synthesis and properties of the first stable neutral germaaromatic compound, 2-{2,4,6-tris[bis(trimethylsilyl)methyl]phenyl}-2-germanaphthalene. Organometallics **22**, 481–489. (e) Takeda, N., Shinohara, A. and Tokitoh, N. (2002) The first stable 9-silaanthracene. Organometallics **21**, 256–258. (f) Sasamori, T., Inamura, K., Hoshino, W., Nakata, N., Mizuhata, Y., Watanabe, Y. *et al.* (2006) Synthesis and characterization of two isomers of 14π-electron germaaromatics: kinetically stabilized 9-germaanthracene and 9-germaphenanthrene. Organometallics **25**, 3533–3536. (g) Tokitoh, N., Shinohara, A., Matsumoto, T., Sasamori, T., Takeda, N. and Furukawa, Y. (2007) Synthesis and properties of a kinetically stabilized 9-silaphenanthrene. Organometallics **26**, 4048–4053.

29) (a) Kinjo, R., Ichinohe, M., Sekiguchi, A., Takagi, N., Sumimoto, M. and Nagase, S. (2007) Reactivity of a disilyne RSi≡SiR (R = $Si^iPr[CH(SiMe_3)_2]_2$) toward π-bonds: stereospecific addition and a new route to an isolable 1,2-disilabenzene. J. Am. Chem. Soc. **129**, 7766–7767. (b) Han, J.S., Sasamori, T., Mizuhata, Y. and Tokitoh, N. (2010) Reactivity of an aryl-substituted silicon–silicon triple bond: 1,2-disilabenzenes from the reactions of a 1,2-diaryldisilyne with alkynes. Dalton Trans. **39**, 9238–9240. (c) Sugahara, T., Guo, J.-D., Hashizume, D., Sasamori, T., Nagase, S. and Tokitoh, N. (2018) The selective formation of a 1,2-disilabenzene from the reaction of a disilyne with phenylacetylene. Dalton Trans. **47**, 13318–13322.

30) (a) Sasamori, T., Sugahara, T., Agou, T., Guo, J.-D., Nagase, S., Streubel, R. *et al.* (2015) Synthesis and characterization of a 1,2-digermabenzene. Organometallics **34**, 2106–2109. (b) Sugahara, T., Guo, J.D., Sasamori, T., Nagase, S. and Tokitoh, N. (2018) Regioselective cyclotrimerization of terminal alkynes using a digermyne. Angew. Chem. Int. Ed. **57**, 3499–3503.

31) Sugahara, T., Sasamori, T. and Tokitoh, N. (2019) The formation of a 1,4-disilabenzene and its isomerization into a disilabenzvalene derivative. Dalton Trans. **48**, 9053–9056.

32) Sugahara, T., Guo, J.D., Hashizume, D., Sasamori, T. and Tokitoh, N. (2019) Reversible isomerizations between 1,4-digermabenzenes and 1,4-digerma-dewar-benzenes: Air-stable activators for small molecules. J. Am. Chem. Soc. **141**, 2263–2267.

33) (a) Saito, M. and Yoshioka, M. (2005) The anions and dianions of group 14 metalloles. Coord. Chem. Rev. **249**, 765–780. For related works on silole anion species, see: (b) Hong, J.H. and Boudjouk, P. (1993) A stable aromatic species containing silicon. Synthesis and characterization of the 1-*tert*-butyl-2,3,4,5-tetraphenyl-1-silacyclopentadienide anion. J. Am. Chem. Soc. **115**, 5883–5884. (c) Goldfuss, B. and Schleyer, P.v.R. (1995) The silolyl anion $C_4H_4SiH^-$ is aromatic and the lithium silolide C_4H_4SiHLi even more so. Organometallics **14**, 1553–1555. For related works on germole anion species, see: (d) Dufour, P., Dubac, J., Dartiguenave, M. and Dartiguenave, Y. (1990) C-methylated (germacyclopentadienyl)lithium. Organometallics **9**, 3001–3003. (e) Freeman, W.P., Tilley, T.D., Arnold, F.P., Rheingold, A.L. and Gantzel, P.K. (1995) Synthesis and Structure of a Free Germacyclopentadienide Anion: $[Li(12\text{-Crown-}4)_2]$ $[C_4Me_4GeSi(SiMe_3)_3]^-$. Angew. Chem. Int. Ed. Engl. **34**, 1887–1890.

34) For related works on silole dianion species, see: (a) Freeman, W.P., Tilley, T.D., Liable-Sands, L.M. and Rheingold, A.L. (1996) Synthesis and study of cyclic π-systems containing silicon and germanium. The question of aromaticity in cyclopentadienyl analogues. J. Am. Chem. Soc. **118**, 10457–10468. (b) Choi, S., Boudjouk, P. and Wei, P. (1998) Aromatic benzannulated silole dianions. The dilithio and disodio salts of a silaindenyl dianion 1. J. Am. Chem. Soc. **120**, 5814–5815. (c) Liu, Y., Stringfellow, T.C., Ballweg, D., Guzei, I.A. and West, R. (2002) Structure and chemistry of 1-silafluorenyl dianion, its derivatives, and an organosilicon diradical dianion. J. Am. Chem. Soc. **124**, 49–57. (d) Liu, Y., Ballweg, D., Müller, T., Guzei, I.A., Clark, R.W. and West, R. (2002) Chemistry of the aromatic 9-germafluorenyl dianion and some related silicon and carbon species. J. Am. Chem. Soc. **124**, 12174–12181. For related works on germole dianion species, see: (e) West, R., Sohn, H., Powell, D.R., Müller, T. and Apeloig, Y. (1996) The dianion of tetraphenylgermole is aromatic. Angew. Chem. Int. Ed. Engl. **35**, 1002–1004. (f) Choi, S., Boudjouk, P. and Hong, J.-H. (1999) Unique bis-η^5/η^1 bonding in a dianionic germole. Synthesis and structural characterization of the dilithium salt of the 2,3,4,5-tetraethyl germole dianion. Organometallics **18**, 2919–2921. (g) Choi, S., Boudjouk, P. and Qin, K. (2000) Aromatic benzannulated germole dianions. The dilithio and disodio salts of a germaindenyl dianion. Organometallics **19**, 1806–1809.

35) Joo, W.-C., Hong, J.-H., Choi, S., Son, H.-E. and Kim, C.H. (1990) Synthesis and reactivity of 1,1-disodio-2,3,4,5-tetraphenyl-1-silacyclopentadiene. J. Organomet. Chem. **391**, 27–36.

36) Hong, J.-H., Boudjouk, P. and Castellino, S. (1994) Synthesis and characterization of two aromatic silicon-containing dianions: The 2,3,4,5-tetraphenylsilole dianion and the 1,1′-disila-2,2′,3,3′,4,4′,5,5′-octaphenylfulvalene dianion. Organometallics **13**, 3387–3389.

37) West, R., Sohn, H., Bankwitz, U., Calabrese, J., Apeloig, Y. and Müller, T. (1995) Dilithium derivative of tetraphenylsilole: An η^1-η^5 dilithium structure. J. Am. Chem. Soc. **117**, 11608–11609.

38) Bankwitz, U., Sohn, H., Powell, D.R. and West, R. (1995) Synthesis, solid-state structure, and reduction of 1,1-dichloro-2,3,4,5-tetramethylsilole. J. Organomet. Chem. **499**, C7–C9.

39) Kanno, K., Ichinohe, M., Kabuto, C. and Kira, M. (1998) Synthesis and structure of a series of oligo[1,1-(2,3,4,5-tetramethylsilole)]s. Chem. Lett. **27**, 99–100.

40) Hong, J.-H. (2017) ^{13}C NMR-Study of 1,1-dipotassio-2,3,4,5-tetraphenyl-1-silacyclopentadienide dianion $[SiC_4Ph_4]^{2-}\cdot 2[K^+]$ and 1,1-dipotassio-2,3,4,5-tetraphenyl-1-germacyclopentadienide dianion $[GeC_4Ph_4]^{2-}\cdot 2[K^+]$. J. Chosun Nat. Sci. **10**, 131–136.

41) Hong, J.-H. and Boudjouk, P. (1995) Synthesis and characterization of a delocalized germanium-containing dianion: Dilithio-2,3,4,5-tetraphenyl-germole. Bull. Soc. Chim. Fr. **132**, 495–498.

42) Ichinohe, M., Igarashi, M., Sanuki, K. and Sekiguchi, A. (2005) Cyclotrisilenylium Ion: The persilaaromatic compound. J. Am. Chem. Soc. **127**, 9978–9979.

43) Sekiguchi, A., Tsukamoto, M. and Ichinohe, M.

(1997) A free cyclotrigermenium cation with a 2π-electron system. Science **275**, 60–61.

44) West, R. (2008) Novel aromatic species containing group 14 atoms. Pure Appl. Chem. **80**, 563–569.

45) Lee, V.Ya., Kato, R., Ichinohe, M. and Sekiguchi, A. (2005) The heavy analogue of CpLi: Lithium 1,2-disila-3-germacyclopentadienide, a 6π-electron aromatic system. J. Am. Chem. Soc. **127**, 13142–13143.

46) (a) Saito, M., Haga, R. and Yoshioka, M. (2002) Formation of the first mono-anion and dianion of stannole. Chem. Commun. (Camb.) 1002–1003. (b) Saito, M., Haga, R. and Yoshioka, M. (2003) Synthesis of stannole anion by alkylation of stannole dianion. Chem. Lett. **32**, 912–913. (c) Saito, M., Haga, R., Yoshioka, M., Ishimura, K. and Nagase, S. (2005) The aromaticity of the stannole dianion. Angew. Chem. Int. Ed. **44**, 6553–6556.

47) Saito, M., Sakaguchi, M., Tajima, T., Ishimura, K., Nagase, S. and Hada, M. (2010) Dilithioplumbole: A lead-bearing aromatic cyclopentadienyl analog. Science **328**, 339–342.

48) (a) Arnold, P.L. and Pearson, S. (2007) Abnormal *N*-heterocyclic carbenes. Coord. Chem. Rev. **251**, 596–609. (b) Crabtree, R.H. (2013) Abnormal, mesoionic and remote *N*-heterocyclic carbene complexes. Coord. Chem. Rev. **257**, 755–766.

49) Mizuhata, Y., Sasamori, T. and Tokitoh, N. (2009) Stable heavier carbene analogues. Chem. Rev. **109**, 3479–3511.

50) (a) Pauling, L. (1960) The Nature of the Chemical Bond, 3rd ed. Cornell University Press, Ithaca, New York. (b) Mulliken, R.S. (1934) A new electroaffinity scale; Together with data on valence states and on valence ionization potentials and electron affinities. J. Chem. Phys. **2**, 782–793. (c) Allred, A.L. (1961) Electronegativity values from thermochemical data. J. Inorg. Nucl. Chem. **17**, 215–221. (d) Sanderson, R.T. (1983) Electronegativity and bond energy. J. Am. Chem. Soc. **105**, 2259–2261. (e) Allen, L.C. (1989) Electronegativity is the average one-electron energy of the valence-shell electrons in ground-state free atoms. J. Am. Chem. Soc. **111**, 9003–9014. (f) Noorizadeh, S. and Shakerzadeh, E. (2008) A New Scale of Electronegativity Based on Electrophilicity Index. J. Phys. Chem. A **112**, 3486–3491.

51) Mizuhata, Y., Fujimori, S., Sasamori, T. and Tokitoh, N. (2017) Germabenzenylpotassium: A germanium analogue of a phenyl anion. Angew. Chem. Int. Ed. **56**, 4588–4592.

52) Fujimori, S., Mizuhata, Y. and Tokitoh, N. (2018) Heavy phenyllithium and -sodium: Synthesis and characterization of germanium analogues of phenyl anion ('Germabenzenyl anions'). Chem. Lett. **47**, 708–710.

53) Tokitoh, N., Matsumoto, T., Suzuki, H. and Okazaki, R. (1991) Unusual 1,3-rearrangement of trimethylsilyl group in the reaction of 2,4,6-tris[bis(trimethylsilyl)methyl]phenyllithium. Tetrahedron Lett. **32**, 2049–2052.

54) For a Review, see: (a) Scheschkewitz, D. (2011) The versatile chemistry of disilenides: Disila analogues of vinyl anions as synthons in low-valent silicon chemistry. Chem. Lett. **40**, 2–11. Disilenyl anions: (b) Weidenbruch, M., Willms, S., Saak, W. and Henkel, G. (1997) Hexaaryltetrasilabuta-1,3-diene: A molecule with conjugated Si-Si double bonds. Angew. Chem. Int. Ed. Engl. **36**, 2503–2504. (c) Scheschkewitz, D. (2004) A silicon analogue of vinyllithium: Structural characterization of a disilenide. Angew. Chem. Int. Ed. **43**, 2965–2967. (d) Ichinohe, M., Sanuki, K., Inoue, S. and Sekiguchi, A. (2004) Disilenyllithium from Tetrasila-1,3-butadiene: A silicon analogue of a vinyllithium. Organometallics **23**, 3088–3090. (e) Inoue, S., Ichinohe, M. and Sekiguchi, A. (2005) Disilenyl anions derived from reduction of tetrakis(di-*tert*-butylmethylsilyl)disilene with metal naphthalenide through a disilene dianion intermediate: Synthesis and characterization. Chem. Lett. **34**, 1564–1565. Digermenyl anions: (f) Park, J., Batcheller, S.A. and Masamune, S. (1989) Synthesis of tetrakis(2,6-diisopropylphenyl)digermene and its reductive cleavage to the corresponding digermenyllithium-(DME) complex. J. Organomet. Chem. **367**, 39–45. (g) Schäfer, H., Saak, W. and Weidenbruch, M. (2000) Hexaaryltetragermabuta-1,3-diene: A molecule with conjugated Ge-Ge double bonds. Angew. Chem. Int. Ed. **39**, 3703–3705.

55) For a Review, see: Saito, M. (2012) Challenge to expand the concept of aromaticity to tin- and lead-containing carbocyclic compounds: synthesis, structures and reactions of dilithiostannoles and dilithioplumbole. Coord. Chem. Rev. **256**, 627–636.

56) Mantina, M., Chamberlin, A.C., Valero, R., Cramer, C.J. and Truhlar, D.G. (2009) Consistent van der Waals radii for the whole main group. J. Phys. Chem. A **113**, 5806–5812.

57) Lee, V.Ya., Sekiguchi, A., Ichinohe, M. and Fukaya, N. (2000) Stable aromatic compounds containing heavier Group 14 elements. J. Organomet. Chem. **611**, 228–235.

58) (a) West, R., Sohn, H., Powell, D.R., Müller, T. and Apeloig, Y. (1996) The dianion of tetraphenylgermole is aromatic. Angew. Chem. Int. Ed. Engl. **35**, 1002–1004. (b) Freeman, W.P., Tilley, T.D., Yap, G.P.A. and Rheingold, A.L. (1996) Silolyl anions and silole dianions: Structure of $[K([18]crown-6)^+]_2[C_4Me_4Si_2^-]$. Angew. Chem. Int. Ed. Engl. **35**, 882–884. (c) Choi, S., Boudjouk, P. and Hong, J.-H. (1999) Unique bis-η^5/η^1 bonding in a dianionic germole. synthesis and structural characterization of the dilithium salt of the 2,3,4,5-tetraethyl germole dianion. Organometallics **18**, 2919–2921. (d) Tandura, S.N., Kolesnikov, S.P., Nosov, K.S., Egorov, M.P. and Nefedov, O.M. (1999) Charge localization in the dianion of tetraphenylgermole according to ^{13}C NMR data. Main Group Met. Chem. **22**, 9–14.

59) (a) Bock, H., Ruppert, K. and Fenske, D. (1989) Tetraphenylethylenedisodium: The band structure

of the CC singly bonded, twisted $(C_6H_5)_2C^{\ominus}$ carbanions. Angew. Chem. Int. Ed. Engl. **28**, 1685–1688. (b) Bock, H., Havlas, Z., Gharagozloo-Hubmann, K., Holl, S. and Sievert, M. (2003) 1,2-Diphenylbenzene dianion: Alkali-metal salts with drastically spread C6 rings. Angew. Chem. Int. Ed. **42**, 4385–4389.

60) Zabula, A.V., Dolinar, B.S. and West, R. (2014) Transformations of spirogermabifluorene upon reduction with alkali metals. J. Organomet. Chem. **751**, 458–461.

61) Hernán-Gómez, A., Herd, E., Uzelac, M., Cadenbach, T., Kennedy, A.R., Borilovic, I. *et al.* (2015) Zincate-mediated arylation reactions of acridine: Pre- and postarylation structural insights. Organometallics **34**, 2614–2623.

62) Breitmaier, E. and Spohn, K.-H. (1973) P_H-abhängigkeit der ^{13}C-chemischen Verschiebungen Sechsgliedriger Stickstoff-heteroaromaten. Tetrahedron **29**, 1145–1152.

63) Elschenbroich, C. (2006) Organometallics, 3rd ed. Wiley-VCH Verlag GmbH & Co. KGaA, Weinheim, Germany.

64) Sekiguchi, A., Sugai, Y., Ebata, K., Kabuto, C. and Sakurai, H. (1993) Lithium pentakis(dimethylsilyl)cyclopentadienide and formation of isolable coordination complexes with ketones: $[(R_2C{=}O)Li{\cdot}\{C_5(SiMe_2H)_5\}]$. J. Am. Chem. Soc. **115**, 1144–1146.

65) Scherr, P.A., Hogan, R.J. and Oliver, J.P. (1974) Correlation of lithium-7 chemical shifts of organolithium derivatives with structural effects. J. Am. Chem. Soc. **96**, 6055–6059.

66) Hong, J.-H., Pan, Y. and Boudjouk, P. (1996) A novel lithocenophane derivative of a trisgermole dianion: $[Li(thf)(tmeda)][2,3,4,5\text{-}Et_4\text{-}Ge,Ge\text{-}\{Li(2,3,4,5\text{-}Et_4C_4Ge)_2\}C_4Ge]$. Angew. Chem. Int. Ed. Engl. **35**, 186–188.

67) (a) Saito, M., Kuwabara, T., Ishimura, K. and Nagase, S. (2010) Synthesis and structures of lithium salts of stannole anions. Bull. Chem. Soc. Jpn. **83**, 825–827. (b) Haga, R., Saito, M. and Yoshioka, M. (2007) Synthesis and reactions of stannole anions. Eur. J. Inorg. Chem. **2007**, 1297–1306.

68) Sasamori, T. and Tokitoh, N. (2005) Group 14 multiple bonding. *In* Encyclopedia of Inorganic Chemistry II (ed. King, R.B.). John Wiley & Sons, Chichester, U.K., pp. 1698–1740.

69) Bourissou, D., Guerret, O., Gabbaï, F.P. and Bertrand, G. (2000) Stable carbenes. Chem. Rev. **100**, 39–92.

70) Trinquier, G. (1990) Double bonds and bridged structures in the heavier analogs of ethylene. J. Am. Chem. Soc. **112**, 2130–2137.

71) Mizuhata, Y., Noda, N. and Tokitoh, N. (2010) Generation of stannabenzenes and their properties. Organometallics **29**, 4781–4784.

72) (a) Tokitoh, N., Takeda, N. and Okazaki, R. (1994) Synthesis and structure of 2,4,6-tris[bis(trimethylsilyl)methyl]thiobenzaldehyde: The first isolation of rotational isomers of thiobenzaldehydes. J. Am. Chem. Soc. **116**, 7907–7908. (b) Takeda, N., Tokitoh, N. and Okazaki, R. (1996) The first rotational isomers of stable selenoaldehydes and their η^1-tungsten complexes. Angew. Chem. Int. Ed. Engl. **35**, 660–662.

73) (a) Mizuhata, Y., Fujimori, S., Noda, N., Kanesato, S. and Tokitoh, N. (2018) Generation of stannabenzenes and their monomer–dimer equilibration. Dalton Trans. **47**, 14436–14444. (b) Fujimori, S., Mizuhata, Y. and Tokitoh, N. (2018) Stannabenzenylpotassium: The first isolable tin-containing benzene derivative. Chem. Eur. J. **24**, 17039–17045.

74) Chen, Z., Wannere, C.S., Corminboeuf, C., Puchta, R. and Schleyer, P.v.R. (2005) Nucleus-independent chemical shifts (NICS) as an aromaticity criterion. Chem. Rev. **105**, 3842–3888.

75) Stanger, A. (2006) Nucleus-independent chemical shifts (NICS): Distance dependence and revised criteria for aromaticity and antiaromaticity. J. Org. Chem. **71**, 883–893.

76) Ashe, A.J., III, Diephouse, T.R. and El-Sheikh, M.Y. (1982) Stabilization of stibabenzene and bismabenzene by 4-alkyl substituents. J. Am. Chem. Soc. **104**, 5693–5699.

77) Ashe, A.J., III (1978) The group 5 heterobenzenes. Acc. Chem. Res. **11**, 153–157.

78) (a) Saito, M., Kuwabara, T., Kambayashi, C., Yoshioka, M., Ishimura, K. and Nagase, S. (2010) Synthesis, structure, and reaction of tetraethyldilithiostannole. Chem. Lett. **39**, 700–701. (b) Kuwabara, T., Guo, J.D., Nagase, S., Minoura, M., Herber, R.H. and Saito, M. (2014) Enhancement of stannylene character in stannole dianion equivalents evidenced by NMR and Mössbauer spectroscopy and theoretical studies of newly synthesized silyl-substituted dilithiostannoles. Organometallics **33**, 2910–2913.

79) Mizuhata, Y., Sasamori, T., Takeda, N. and Tokitoh, N. (2006) A stable neutral stannaaromatic compound: Synthesis, structure and complexation of a kinetically stabilized 2-stannanaphthalene. J. Am. Chem. Soc. **128**, 1050–1051.

80) Glendening, E.D., Landis, C.R. and Weinhold, F. (2013) NBO 6.0: Natural bond orbital analysis program. J. Comput. Chem. **34**, 1429–1437.

81) Mizuhata, Y., Fujimori, S. and Tokitoh, N. (2020) Reaction of germabenzenylpotassium with TBDMSCl: Unusual trimerization of germabenzene skeletons. Phosphorus Sulfur Silicon Relat. Elem. **195**, 936–939.

82) (a) Tokitoh, N., Manmaru, K. and Okazaki, R. (1994) Synthesis of novel aryl-substituted germylenes by steric protection and their reactions. Nippon Kagaku Kaishi 240–247 (in Japanese with English abstract). (b) Baines, K.M., Cooke, J.A., Dixon, C.E., Liu, H.W. and Netherton, M.R. (1994) Thermolysis of hexamesitylsiladigermirane or hexamesitylcyclotrigermane in the presence of 2,3-dimethylbutadiene or water. Organometallics **13**, 631–634. (c) Leigh, W.J., Harrington, C.R. and Vargas-Baca, I. (2004) Organogermanium

reactive intermediates. The direct detection and characterization of transient germylenes and digermenes in solution. J. Am. Chem. Soc. **126**, 16105–16116.

83) Lee, V.Ya. and Sekiguchi, A. (2008) Cyclic polyenes of heavy group 14 elements: New generation ligands for transition-metal complexes. Chem. Soc. Rev. **37**, 1652–1665.

84) (a) Dysard, J.M. and Tilley, T.D. (1998) η^5-Silolyl and η^5-germolyl complexes of d^0 hafnium. Structural characterization of an η^5-silolyl complex. J. Am. Chem. Soc. **120**, 8245–8246. (b) Freeman, W.P., Don. Tilley, T. and Rheingold, A.L. (1994) Stable silacyclopentadienyl complexes of ruthenium: (η^5-C_5Me_5)Ru[η^5-$Me_4C_4SiSi(SiMe_3)_3$] and X-ray structure of its protonated form. J. Am. Chem. Soc. **116**, 8428–8429.

85) (a) Freeman, W.P., Tilley, T.D., Rheingold, A.L. and Ostrander, R.L. (1993) A stable η^5-germacyclopentadienyl complex: [($\eta^5C_5Me_5$)Ru{η^5-C_4Me_4-$GeSi(SiMe_3)_3$}]. Angew. Chem. Int. Ed. Engl. **32**, 1744–1745. (b) Freeman, W.P., Dysard, J.M., Tilley, T.D. and Rheingold, A.L. (2002) Synthesis and reactivity of η^5-germacyclopentadienyl complexes of iron. Organometallics **21**, 1734–1738.

86) Yasuda, H., Lee, V.Ya. and Sekiguchi, A. (2009) η^5-1,2,3-Trisilacyclopentadienyl − A ligand for transition metal complexes: Rhodium half-sandwich and ruthenium sandwich. J. Am. Chem. Soc. **131**, 9902–9903.

87) (a) Lee, V.Ya., Kato, R., Sekiguchi, A., Krapp, A. and Frenking, G. (2007) Heavy ferrocene: A sandwich complex containing Si and Ge atoms. J. Am. Chem. Soc. **129**, 10340–10341. (b) Lee, V.Ya., Kato, R. and Sekiguchi, A. (2013) Heavy metallocenes of the group 8 metals: Ferrocene and ruthenocene derivatives. Bull. Chem. Soc. Jpn. **86**, 1466–1471.

88) (a) Kuwabara, T., Guo, J.D., Nagase, S., Sasamori, T., Tokitoh, N. and Saito, M. (2014) Synthesis, structures, and electronic properties of triple- and double-decker ruthenocenes incorporated by a group 14 metallole dianion ligand. J. Am. Chem. Soc. **136**, 13059–13064. (b) Kuwabara, T. and Saito, M. (2015) Synthesis of a stannole dianion complex bearing a μ-η^1;η^1-coordination mode: different electronic state of stannole dianion ligands depending on their hapticity. Organometallics **34**, 4202–4204.

89) Nakada, M., Kuwabara, T., Furukawa, S., Hada, M., Minoura, M. and Saito, M. (2017) Synthesis and reactivity of a ruthenocene-type complex bearing an aromatic π-ligand with the heaviest group 14 element. Chem. Sci. **8**, 3092–3097.

90) Kon, Y., Sakamoto, K., Kabuto, C. and Kira, M. (2005) A cobalt silacyclobutadiene complex. Organometallics **24**, 1407–1409.

91) Takanashi, K., Lee, V.Ya., Ichinohe, M. and Sekiguchi, A. (2007) (η^5-Cyclopentadienyl)(η^4-tetrasila- and η^4-trisilagermacyclobutadiene)cobalt: Sandwich complexes featuring heavy cyclobutadiene ligands. Eur. J. Inorg. Chem. **2007**, 5471–5474.

92) (a) Takanashi, K., Lee, V.Ya., Matsuno, T., Ichinohe, M. and Sekiguchi, A. (2005) Tetrasilacyclobutadiene ($t$$Bu_2MeSi)_4Si_4$: A new ligand for transition-metal complexes. J. Am. Chem. Soc. **127**, 5768–5769. (b) Takanashi, K., Lee, V.Ya., Ichinohe, M. and Sekiguchi, A. (2006) A (Tetrasilacyclobutadiene)tricarbonyliron Complex [{η^4-($t$$Bu_2MeSi)_4Si_4$}$Fe(CO)_3$]: The silicon cousin of Pettit's (cyclobutadiene)tricarbonyliron complex [(η^4-H_4C_4)$Fe(CO)_3$]. Angew. Chem. Int. Ed. **45**, 3269–3272. (c) Takanashi, K., Lee, V.Ya. and Sekiguchi, A. (2009) Tetrasilacyclobutadiene and cyclobutadiene tricarbonylruthenium complexes: [η^4-($t$$Bu_2MeSi)_4Si_4$]$Ru(CO)_3$ and [h^4-$(Me_3Si)_4$-C_4]$Ru(CO)_3$. Organometallics **28**, 1248–1251. (d) Lee, V.Ya., Takanashi, K. and Sekiguchi, A. (2010) A two-and-a-half-layer sandwich: potassium salt of anionic (η^4-tetrasilacyclobutadiene)(η^5-cyclopentadienyl)ruthenium. Dalton Trans. **39**, 9229–9231.

93) (a) Lee, V.Ya., Ito, Y. and Sekiguchi, A. (2013) (Tetragermacyclobutadiene)ruthenium tricarbonyl [η^4-$(But_2MeSi)_4Ge_4$]$Ru(CO)_3$. Russ. Chem. Bull. **62**, 2551–2553. (b) Lee, V.Ya., Ito, Y., Yasuda, H., Takanashi, K. and Sekiguchi, A. (2011) From tetragermacyclobutene to tetragermacyclobutadiene dianion to tetragermacyclobutadiene transition metal complexes. J. Am. Chem. Soc. **133**, 5103–5108.

94) (a) Shinohara, A., Takeda, N., Sasamori, T., Matsumoto, T. and Tokitoh, N. (2005) Synthesis and properties of η^6-silabenzene–$M(CO)_3$ complexes (M = Cr, Mo). Organometallics **24**, 6141–6146. (b) Tanabe, Y., Mizuhata, Y. and Tokitoh, N. (2008) Mechanistic investigation of the hydration reaction of [Cr(η^6-silabenzene)$(CO)_3$]: Hydrido(silacyclohexadienyl)chromium complex as an intermediate. Chem. Lett. **37**, 720–721. (c) Nakata, N., Takeda, N. and Tokitoh, N. (2003) η^6-Germabenzene complexes of chromium and molybdenum. Angew. Chem. Int. Ed. **42**, 115–117. (d) Tokitoh, N., Nakata, N., Shinohara, A., Takeda, N. and Sasamori, T. (2007) Coordination chemistry of a kinetically stabilized germabenzene: syntheses and properties of stable η^6-germabenzene complexes coordinated to transition metals. Chemistry **13**, 1856–1862. (e) Mizuhata, Y., Sasamori, T., Takeda, N. and Tokitoh, N. (2006) A stable neutral stannaaromatic compound: Synthesis, structure and complexation of a kinetically stabilized 2-stannanaphthalene. J. Am. Chem. Soc. **128**, 1050–1051.

95) Fujimori, S., Mizuhata, Y. and Tokitoh, N. (2018) Ru-Complexes of an anionic germabenzenyl ligand. Chem. Commun. (Camb.) **54**, 8044–8047.

96) (a) Zhang, Y., Wang, B., Xu, S. and Zhou, X. (2001) Unexpected formation of the ruthenium carbonyl cluster with a trigonal-bipyramidal Ge_2Ru_3 core accompanied by loss of germanium methyl groups. Organometallics **20**, 3829–3832. (b) Albertin, G., Antoniutti, S., Castro, J. and Scapinello, F. (2014)

Preparation and reactivity of germyl complexes of ruthenium and osmium stabilised by cyclopentadienyl, indenyl and tris(pyrazolyl)borate fragments. J. Organomet. Chem. **751**, 412–419.

97) (a) Urbanos, F., Halcrow, M.A., Fernandez-Baeza, J., Dahan, F., Labroue, D. and Chaudret, B. (1993) Selective aromatization of the A-Ring of steroids through carbon-carbon, carbon-hydrogen, and carbon-oxygen bond activation by an electrophilic ruthenium complex. J. Am. Chem. Soc. **115**, 3484–3493. (b) Volbeda, J., Daniliuc, C.G., Jones, P.G. and Tamm, M. (2013) Half-open ferrocenes and ruthenocenes containing an edge-bridged open indenyl ligand. Organometallics **32**, 5918–5925. (c) Mohapatra, S.K., Fonari, A., Risko, C., Yesudas, K., Moudgil, K., Delcamp, J.H. *et al.* (2014) Dimers of nineteen-electron sandwich compounds: Crystal and electronic structures, and comparison of reducing strengths. Chem. Eur. J. **20**, 15385–15394.

98) (a) Barsuaskas, G., Lei, D., Hampden-Smith, M.J. and Duesler, E.N. (1990) The first evidence for reductive coupling of transition metal substituted halogermanes. Polyhedron **9**, 773–776. (b) Sen, S.S., Kratzert, D., Stern, D., Roesky, H.W. and Stalke, D. (2010) Reactivity studies of a Ge^{I}-Ge^{I} compound with and without cleavage of the Ge-Ge bond. Inorg. Chem. **49**, 5786–5788.

(Received July 19, 2023; accepted Sep. 25, 2023)

Profile

Shiori Fujimori received her M.Sc. and Ph.D. degrees in chemistry in 2019 from Kyoto University under the supervision of Prof. Norihiro Tokitoh on the synthesis of novel aromatic compounds containing heavier Group 14 element. While at Kyoto University, Dr. Fujimori won the "TOBITATE! Young Ambassador Program" scholarship, which allowed her to first travel to Canada as a researcher. In 2017, she spent six months working as a visiting research fellow in the research group of Prof. Eric Rivard at the University of Alberta. She received many student awards, including the "2018 Kyoto University TACHIBANA Award for Outstanding Women Researchers", which acknowledges the excellent achievements of early-career female researchers at Kyoto University. In October 2019, she was awarded a Eurotech-Marie Curie Fellowship and joined the group of Prof. Shigeyoshi Inoue at TU München, Germany. She is continuing her stay at TU München as an Alexander von Humboldt Fellow, where she pursued her interest in low-valent silicon chemistry.

Profile

Yoshiyuki Mizuhata was born in 1977. He received his B.Sc. (2001), M.Sc. (2003), and Ph.D. (2006) degrees from Kyoto University, Japan. He worked as a Research Fellow of the Japan Society for the Promotion of Science (JSPS) (2005–2006) and Assistant Professor (2006–2017) at the Institute for Chemical Research, Kyoto University. He has been an Associate Professor at the Institute for Chemical Research, Kyoto University, since 2017. His main research fields are organometallic and main-group-element chemistry. He received the Inoue Research Award for Young Scientists (2007); the Mitsubishi Chemical Co., Ltd., Award in Synthetic Organic Chemistry of Japan (2008); the Progress Award in Silicon Chemistry, Japan (2016); and the Kansai Branch Award of the Society of Synthetic Organic Chemistry, Japan (2019).

Profile

Norihiro Tokitoh was born in Miyazaki Prefecture in 1957 and graduated from The University of Tokyo in 1979. He received his Ph.D. degree from the Graduate School of Science, The University of Tokyo (1985). He started his academic career as an Assist. Prof. of Tsukuba University (1987) and then as an Assist. Prof. (1989) and Assoc. Prof. (1994) of The University of Tokyo. In 1998, he was promoted as a Professor of the Institute of Fundamental Organic Chemistry, Kyushu University, and in 2000, he moved to the Institute for Chemical Research (ICR), Kyoto University, where he served as a Professor until 2022. Since 2020, he has been the Executive Vice-President of Kyoto University. During his career, he served as Guest Professor, Institute for Molecular Science (2001–2003); Visiting Professor, TU Braunschweig (2004–2007) and Universität Bonn (2013–2015); Director of ICR (2008–2012 and 2014–2018); Dean, Division of Natural Sciences, Kyoto University (2016–2018); Director, Section of Integrated Chemistry, Kyoto University (2016–2018); Director, Kyoto University Research Coordination Alliance (2018–2020); and Director, Center for the Promotion of Interdisciplinary Education and Research, Kyoto University (2022–present). Furthermore, he served as the President of the Society of Silicon Chemistry, Japan (2016–2018), and The Society of Physical Organic Chemistry, Japan (2018–2022), in addition to his contribution as an international advisory board member of many international academic societies. He has conducted pioneering and challenging research toward the creation of unexplored molecules of heavier main group elements. For his accomplishments, he received many awards and honors, such as Japan IBM Science Award (1998), Chemical Society of Japan Award for Creative Work (2003), Alexander von Humboldt Research Award (2003 and 2013), The Society of Silicon Chemistry Award (2019), The Chemical Society of Japan Award (2021), and Japan Physical Organic Chemistry Award (2023).